ABSTRACT

DAVIES, JUBRIL AJIBOLA. A Seismo-Acoustic Investigation of Microseismicity in the Lau Basin. (Under the direction of: DelWayne Bohnenstiehl).

A long-standing challenge in monitoring of mid-ocean ridge seismicity has been the accuracy of earthquake locations. Both ocean bottom seismometer (OBS) and autonomous underwater hydrophone (AUH) arrays can be used to detect and locate mid-ocean ridge seismicity. In this study, a comparison of 375 earthquakes located using both hydrophone recorded T-waves and local seismic P and S phases is made for events associated with the Eastern Lau Spreading Center (ELSC), a back-arc rift zone within the Western Pacific. We find that in general the epicenters derived using local seismic phases agree with the T-wave derived source locations. Uncertainties in epicenter location are evaluated using a two-sigma confidence ellipse as determined by the covariance matrix of the weighted least squares formulation. OBS derived locations have uncertainties between 1.67 km and 2.03 km while T-wave epicenters have uncertainties between 1.32 km and 1.72 km. For events on the off-axis flanks of the ELSC, 57% of the T-wave derived epicenters fall within the 95% confidence region of the seismic derived epicenters, as opposed to 46% for earthquakes along the spreading axis. However, the confidence limits of OBS and AUH derived locations overlap for about 87% of off-axis seismo-acoustic event pairs and 89% of along-axis event pairs. We also note a mean origin time difference between OBS and AUH derived epicenters of 2.63±0.90seconds for events off the axis and 3.03±0.15 seconds for earthquakes along the axis. This delay represents the time it takes seismic energy leaving the earthquake focus to couple into the sound channel as an acoustic wave. Due to the array geometries, T-wave source locations are located to the southwest of the seismic epicenter for events on-axis and

to the southeast for events off-axis. This observation is no indication that T-wave epicenters are biased toward regions of shallower topography. Earthquakes with magnitudes as low as ML 1.0 have been recorded with source levels as low as 179.4 dB re 1 mPa @ 1 m. Acoustic source level and magnitude are linearly correlated with R^2=0.59 for on axis earthquakes and R^2=0.46 for off-axis earthquakes.

A Seismo-Acoustic Investigation of Microseismicity in the Lau basin

by
Jubril Ajibola Davies

A thesis submitted to the Graduate Faculty of
North Carolina State University
in partial fulfillment of the
requirements for the degree of
Master of Science

Marine, Earth & Atmospheric Sciences

Raleigh, North Carolina

2014

APPROVED BY:

_____	_____
Karl Wegmann	James Hibbard

_____
DelWayne Bohnenstiehl
Chair of Advisory Committee

DEDICATION

I would like to dedicate this degree to Almighty Allah for seeing me through the trying periods of my academic program and giving me the strength to complete the program. I would also like to show dedication to both of my parents who supported me with their prayers both night and day. They have been more than a source of strength but a motivation as well.

BIOGRAPHY

Jubril Davies was born and raised in Lagos, Nigeria where he studied Chemical Engineering at the University of Lagos, Nigeria. He worked as a Project Engineer for a while with an Environmental Consulting company in Nigeria before deciding to pursue Graduate studies in Earth Sciences where he developed passion for Geophysics. He continued graduate studies at North Carolina State University, Raleigh where he focused on Marine Geology and geophysics. He aspires to be an Industry-based professional researching and contributing to the development of energy and mineral resources in the Oil and Natural Gas Industry.

ACKNOWLEDGMENTS

I acknowledge my Advisor, Dr Delwayne Bohnenstiehl for his support, advice and patience through my academic program. He has chiseled me into the professional geoscientist that I am today. I would also like to thank my committee members Dr Karl Wegmann and Dr Jim Hibbard for their contributions. I also acknowledge the faculty and staff of the Marine, Earth & atmospheric sciences for their hospitality and kindness during my stay at North Carolina State University. In one way or the other, everyone has played a role in my success in this program. This work was supported by the National Science Foundation grants OCE-0825295.

TABLE OF CONTENTS

LIST OF TABLES

LIST OF FIGURES

INTRODUCTION

1.1 THE STATE OF HYDROACOUSTIC MONITORING

This thesis is focused on a geophysical investigation utilizing the principles of seismology and hydroacoustics in constraining the seismotectonics of the Lau basin. The Lau basin is located in the southwest Pacific Ocean and is an evolving back arc system. Assessing the uncertainty in earthquake locations is critical in making accurate tectonic interpretations. A comparison of two methods of earthquake location is made feasible using ocean-bottom seismic and sound-channel based hydroacoustic observations obtained contemporaneously along the Eastern Lau Spreading Center (ELSC) over a five month period in late 2009 and early 2010.

Hydroacoustics has been used extensively in the past as a long term monitoring tool in constraining models of the mid-ocean ridge tectonics (Dziak et al., 2004, Bohnenstiehl et al., 2002, 2003). Studies have tried to correlate the acoustic source level with seismic magnitude with the aim of deriving an acoustic magnitude from Tertiary (T) -wave arrivals. But estimation of low magnitude (ML < 4.0) events has been hampered by the distance of land-based seismic stations to the epicenters of submarine earthquakes, as well as limited coverage of Ocean Bottom Seismometer (OBS) arrays on the seafloor. Hydroacoustic studies take advantage of the quasi-cylindrical spreading property of the Sound Fixing And Ranging (SOFAR) channel (Tolstoy and Ewing, 1950). In the past, the T-wave from earthquakes as small as magnitude ~1.8 have been detected in remote ocean areas at ranges of several

hundreds of kilometers (Slack et al., 1999). Despite the proliferation of T-wave studies over the last few decades, much is still unknown about T-wave event characteristics and their relationship to earthquake properties. When a submarine earthquake occurs beneath the seafloor, the seismic energy crossing the seafloor interface couples into the water column over some area of the seafloor surrounding the epicenter [Slack et al., 1999, Yang & Forsyth 2003]. This introduces an uncertainty in the estimated source location, as it is not a true point source, and in some instances the site of acoustic coupling may not represent the true epicenter of the earthquake [e.g., Tolstoy, M. and D.R. Bohnenstiehl, 2004]. The seismo-acoustic coupling mechanism, which explains the conversion of seismic energy at the seafloor into acoustic energy in the sound channel, is still not well understood. Several models have been proposed to explain the horizontal propagation and entrapment of the T-wave in the sound channel. These include down-slope conversion (Tolstoy and Ewing, 1950), seafloor-surface reflection scattering (Johnson et al., 1967) and seafloor reflection roughness scattering (Fox et al, 1994).

Previous attempts have been made at examining the correlation between T-wave epicenters derived from moored hydrophone recordings and seismic epicenters derived from analysis of solid earth seismic phases recorded at teleseismic distances. Bohnenstiehl and Tolstoy (2003) compared the estimated location of T-wave events along the equatorial East Pacific Rise and northern Mid-Atlantic Ridge with those published within the International Data Centre's (IDC) Reviewed Event Bulletin (REB). They showed that the offset in distance between the epicenters derived using land-based seismic stations and AUH's (Autonomous Underwater

Hydrophones) decreases as the number of seismic stations detecting the event increases and the maximum azimuthal gap (largest distance between stations recording a quake - USGS) between the epicenter and these stations decreases. This study argues for the increased accuracy of T-wave epicenters within remote oceanic areas, in relation to global seismic catalogs, and emphasizes the need for good azimuthal coverage of seismic stations. Pan and Dziewonski (2005) later compared T-wave derived epicenters along the Mid-Atlantic ridge with a set of relocated seismic epicenters and the moment centroid positions of $m_b > 5.5$ earthquakes. They noted that the locations of T-wave derived epicenters were positioned between the hypocenter and moment centroid position and confined within the estimated errors of the seismic locations.

Williams et al. (2006) investigated the potential for bathymetric steering of T-wave source locations toward the crests of two shallow massifs near the Atlantis (30^oN) and Kane ($23^o40'N$) Transform on the Mid-Atlantic Ridge. A greater number of T-wave events (ML > 2.5-3.0) were located on the massifs at seafloor depths of 1 – 2 km, compared to the surrounding seafloor. In a later study involving five short-period OBS instruments deployed at the Atlantis Massif, Collins et al. (2012) showed that the majority of the ML > 2.5 earthquakes at the time of their investigation were located within the axial valley. Both studies, in conclusion, called for a concurrent seismo-acoustic investigation. To investigate potential disparity between the two earthquake location methods, we utilize data from a dense array of 51 ocean bottom seismometers along with 6 autonomous underwater hydrophone stations monitoring a 125 km long section of the ELSC. The availability of a

100m resolution grid multibeam data along the length of ELSC with higher resolution DSL-120 (5m) bathymetry data along the youngest portion of the seafloor (Martinez et al., 2006) affords us the opportunity to identify location bias associated with small-scale topography.

This study is among the first efforts at undertaking the concurrent monitoring of small magnitude earthquakes using both sound-channel based hydroacoustic and ocean bottom seismic observations. This thesis allows for understanding the relationship between T-wave event characteristics and earthquake properties at low magnitude scales. By examining the spatio-temporal distribution of T-wave event locations in relation to seismic events, we assess the variability of some T-wave characteristics over the duration of the study.

1.2 GEOACOUSTIC SETTING OF THE LAU BASIN

The Lau back-arc basin is located in the southwest Pacific Ocean where the Pacific plate is subducting beneath the Tofua Arc at the Tonga Trench. It is bounded by Tofua arc to the west and Lau ridge (remnant arc) to the east (Fig.1). Crustal accretion and seafloor spreading takes place in the eastern part of the basin along the Eastern Lau Spreading Center. This is a 400km long spreading center that marks the boundary between the Australian and Tonga plate. Investigating the shallow seismicity associated with tectonic strain in this region will improve our understanding of the evolving seismo-tectonic of the basin (Zellmer and Taylor, 2001).

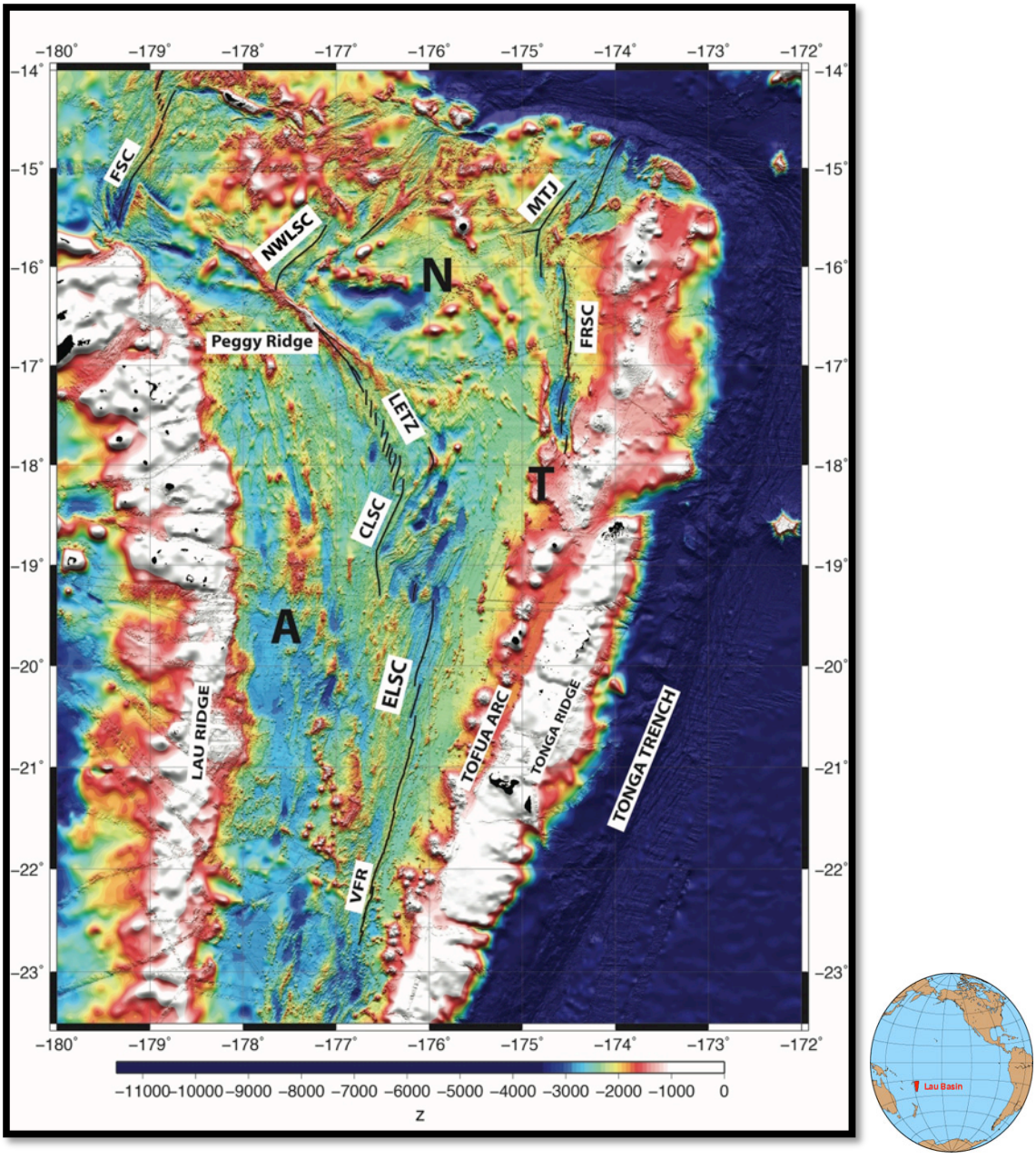

Figure 1. Bathymetric map of Lau Basin. Lines are spreading center traces. MTJ = Mangatolu Triple Junction, FSC = Futuna Spreading Center, NWLSC = Northwest Lau Spreading Center, FRSC = Fonulei Ridge Spreading Center, LETZ = Lau Extensional Transform Zone, ELSC = Eastern Lau Spreading Center and CLSC = Central Lau Spreading Center. A = Australian plate, T = Tonga plate, N = Nioufou plate. Data compilation is courtesy of F. Martinez.

The sound velocity profile of the Lau Basin is shown in Figure 2. The velocity at the sea surface is about 1540m/s and it is at a minimum at about 1420m/s at about 1100m depth. At this depth lies the sound channel axis and the depth at which the sound velocity is the same as that of the sea surface is known as the critical depth. The Lau Basin's ocean acoustic environment is bottom limited implying that the critical depth of the sound channel (~5500m) lies below the average depth of the seafloor (~2360m) (Fig.2). Depending on the local depth, slope and aspect of the seafloor, these bottom interacting signals may become entrapped in the sound fixing and ranging (SOFAR) channel (Ewing and Worzel, 1948), where they propagate with minimal transmission loss for very long distances (Tolstoy and Ewing, 1950; Ulrick, 1983). Scattering is herein invoked as the principal mechanism of T-wave excitation due to the roughness and heterogeneity of the seafloor boundary (Bradley and Stephen, 1996; Park et al., 2001). This process serves to re-radiate some portion of the incident seismic energy into a nearly horizontally propagating acoustic energy (Figure 2).

For a T-wave generated from an earthquake source in the oceanic crust and upper mantle, a hydroacoustic wave gets excited at the seafloor-ocean interface and travels at the speed of sound in water (~1.5 km/s). The T-wave arrives after the faster traveling P- (Primary) and S- (Secondary) body waves, which propagate through the earth (Tolstoy and Ewing, 1950; Johnson et al., 1963). The T-wave acoustic energy occurs within a frequency band of 1 – 100Hz. The spectrogram is characterized by an envelope where the amplitude of the wave rises to a maximum prior to decaying to ambient noise levels (Figure 3). For shallow earthquakes, Slack et. al (1999) proposed that the maximum amplitude of the T-wave

envelope corresponds energy generated above the hypocenter, where the amplitude of T-wave excitation is expected to be greatest.

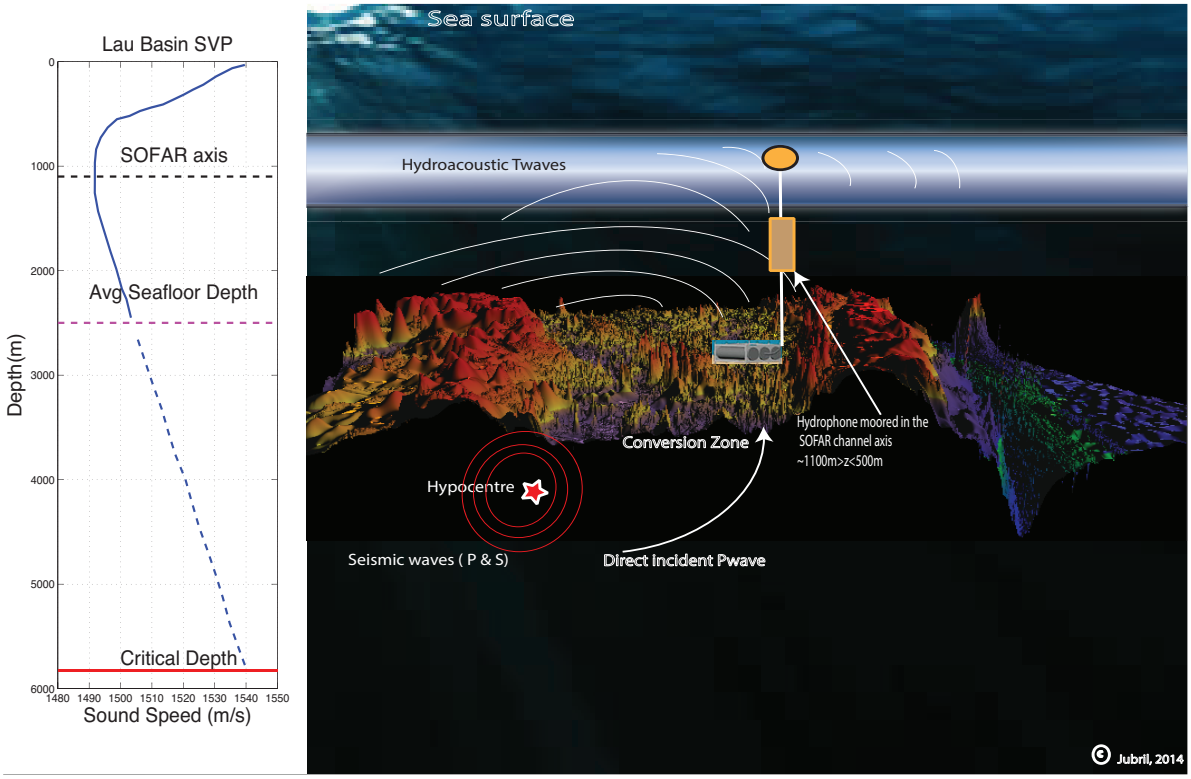

Figure 2: Schematic illustration of T-wave Excitation & Propagation from an earthquake source**.** (Left) Lau basin sound velocity profile. Average seafloor depth at (~2500m) and Critical depth at (~5500m).

2.0 EARTHQUAKE LOCATION METHODS

2.1 PROCESSING SEISMIC DATA WITH ANTELOPE

Ocean bottom seismic data are processed using the Antelope software suite. Antelope provides a relational database system to organize metadata, waveforms, event detections, arrival times of seismic phases and earthquake parameters. With built-in library routines, it offers the applications for event detection, event association, arrival time picking and location of seismic events. Figure 3 shows a schematic representation of the generalized processing scheme used.

All waveform files are linked to the channels on which they were recorded (station name, location, and sensor component) using **miniseed2db** application in Antelope. Potential arrival times of seismic P-phases are then compiled by running the program **dbdetect**; this program computes a short-term-average/long-term-average ratio across the vertical channel waveforms and declares a detection when the ratio exceed a given threshold. In this study, we adopt a threshold of 3.5 and operated the detector using a 5-Hz high pass filtered version of the waveforms. These detections are then associated using a grid-search routine, **dbgrassoc**, with a minimum of five detections across the network necessary to form an event. The initial travel-time calculations assume the IASP91 velocity model. P and S arrival times identified using the detection and association procedure were reviewed manually on seismograms using **dbpick** and **dbloc2** interface in the Antelope waveform-processing suite.

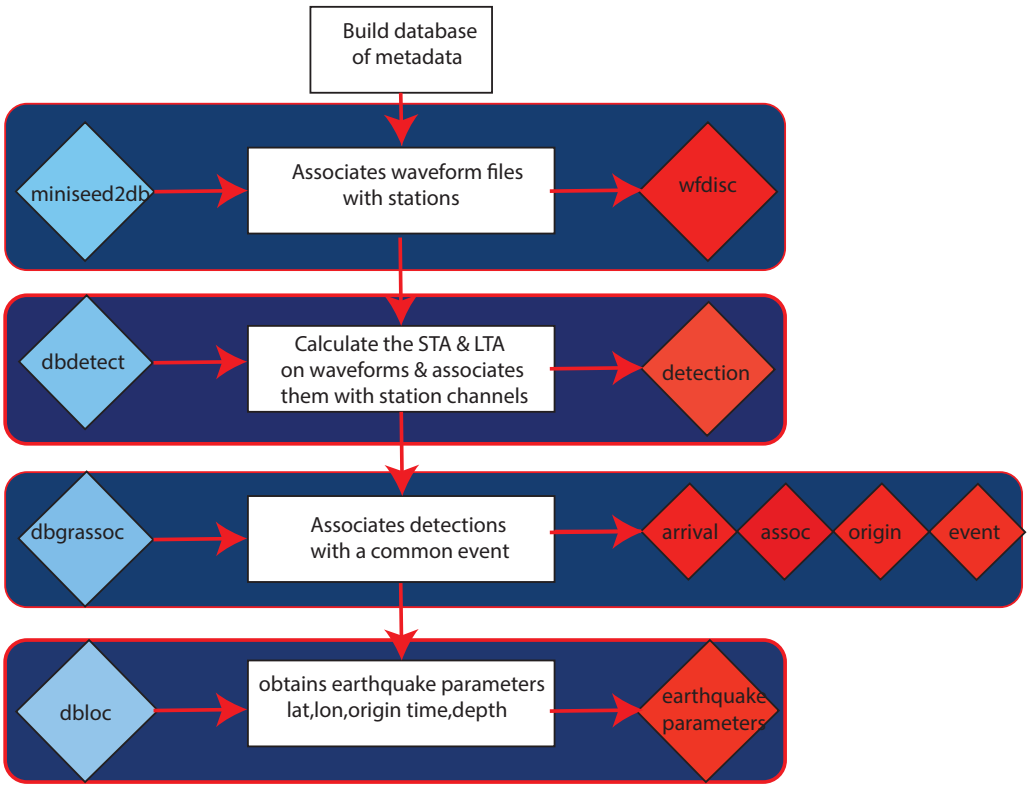

Figure 3: Antelope generalized processing scheme. The workflow starts with the building of the seismic event database based on CSS 3.0 schema. Blue diamonds represents programs and respective processes are written in rectangular boxes. Red diamonds depicts the result of such processes.

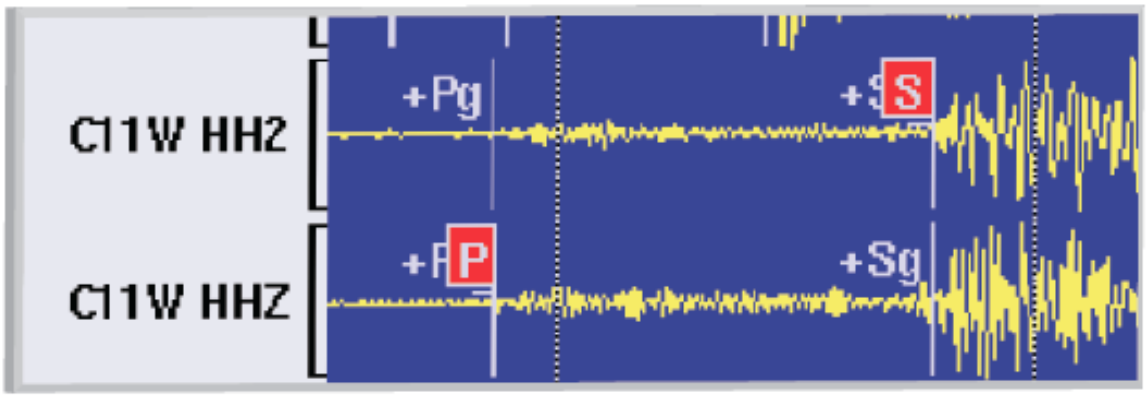

Figure. 4 Seismogram recorded by an Ocean bottom seismometer within a local distance of a seismic event within the Lau basin. Predicted P and S arrival times are shown as +Pg and Sg respectively. The arrival times picked by the analyst are flagged as P on vertical channels and S on horizontal channels. HHZ and HH2 represent both the vertical and horizontal channels of the station C11W. Stations suffixed with W represent WHOI (Woods-Hole Institution stations).

2.2 EVENT RELOCATION WITH HYPOINVERSE

Analyst-reviewed arrivals from a well-recorded subset of events were then relocated in Hypoinverse using the velocity model of the Eastern Lau Spreading Center obtained from a recent active source tomographic experiment described in (Dunn et.al 2013). Within Hypoinverse, the absolute locations of earthquakes are derived by minimizing the weighted squares of the residuals between the 1-D predicted and observed travel times (Klein, 2002). Hypoinverse is based on the Geiger algorithm and it involves solving for the hypocentral parameters in a least square sense using the single value decomposition method. The covariance matrix of eigenvalues reports the errors in the solution (i.e. the largest error in the horizontal and vertical direction).

2.2.1 THE CRUSTAL VELOCITY MODEL

The crustal velocity model of the study area is a key factor influencing the positioning accuracy as well as the accuracy of phase identification, picking of arrival times and the network layout. In this study, we built the crustal model (shown in Table 1) based on the results from active source wide-angle reflection/refraction profile carried out by Dunn et.al (2013). A constant P-to-S wave ratio of 1.78 was used. This value was estimated by averaging the slopes of obtained from a series of Wadati plots for each earthquake having more than four P-S arrival pairs.

Table 2.1 Velocity Model used in Hypoinverse

Layer number	Interface top depth/km	P-wave velocity/ (km/s)
1	0	2.26
2	0.34	2.70
3	0.67	3.66
4	1.01	4.40
5	1.34	4.81
6	1.68	5.18
7	2.01	5.56
8	2.35	5.95
9	2.68	6.30
10	3.02	6.51
11	3.35	6.67
12	3.69	6.81
13	4.02	6.91
14	4.36	7.01
15	4.69	7.07
16	5.03	7.10
17	5.36	7.11
18	5.70	7.13
19	6.00	7.20
20	8.05	7.80

2.3 SEISMIC MAGNITUDE CALCULATIONS

This study focuses on local earthquakes occurring within the basin. Local earthquake magnitude ML is calculated using the standard IASPEI attenuation model (Bormann, 2012):

$$ML = \log_{10}(A) + 1.11 \log_{10}R + 0.00189*R - 2.09$$

where A = maximum trace amplitude in nm that is measured on output from a horizontal-component instrument that is filtered so that the response of the seismograph/filter system replicates that of a Wood-Anderson standard seismograph but with a static magnification of 1. R is the hypocentral distance in km.

2.4 HYDROACOUSTIC DATA PROCESSING

In the January of 2009, an array of six moored hydrophone stations was deployed along on the Eastern Lau Spreading Center between ~ 17◦S and 23◦S, presenting an opportunity to detect and locate moderate size, shallow-hypocenter earthquakes within this evolving plate boundary region. This array overlaps spatially and temporally with a dense network of 51 ocean bottom seismometers. Each acoustic instrument consists of a single hydrophone sensor floated within the sound channel axis at a depth of ~ 1000±50 m and tethered via an acoustic release to a seafloor anchor. The recording unit consists of a filter/amplifier stage designed to pre-whiten the ambient noise spectrum, an accurate (< 1 s per year drift) clock that is GPS-synchronized prior to deployment, a logging computer, and multiple hard disks for data storage. The systems were programmed to record 2-byte resolution at a sample rate of 250 Hz. One of the hydrophone stations consisted of a short baseline four-element horizontal

array, which was incorporated to provide azimuthal detection information [e.g., Bohnenstiehl, D.R., R. P. Dziak, H. Matsumoto, J. Conder, 2014], and another consisted of a three-element vertical array to investigate variability in T-wave amplitude with depth [e.g., H. Matsumoto; D.R. Bohnenstiehl; R.P. Dziak; L. Williams; R. Gliege; C.N. Meinig; P. Harben, A vertical hydrophone array coupled via inductive modem for detecting deep-ocean seismic and volcanic sources MTS/IEEE Seattle, OCEANS 2010 2010]. Only data collected between November 2009 and April 2010, when the AUH and OBS arrays were deployed at the same time, are considered in this thesis.

An analyst picks T-wave arrival times by identifying the peak in the T-wave envelope or spectrogram (Fig. 5). The correlation of event depth and rise time in the abyssal setting suggests that this portion of the signal radiates from the near epicentral region, where the amplitude of the scattered energy is largest (Dziak et al., 1995; Slack et al., 1999). The hydroacoustic source location and origin time are derived using an iterative nonlinear least-squares method that minimizes the squared differences between the predicted and recorded arrival times at each instrument. This procedure is implemented within NOAA's SEASICK software, as described in Fox et al. (2001). Hydroacoustic travel times are calculated within a sound speed model derived from the Generalized Digital Environmental Model (GDEM) (Teague et al., 1990). After each event is located, an independent estimate of the acoustic magnitude, or source level (SL), is calculated for each receiving hydrophone by adding a transmission loss factor that accounts for both spherical spreading from the seafloor into the sound channel and cylindrical spreading along the sound channel path (Fox et al., 2001). Source levels are measured in decibels relative to 1μPa at 1m (dB re_μPa @ 1m) (Dziak et

al., 1997; Dziak, 2001; Fox et al., 2001).

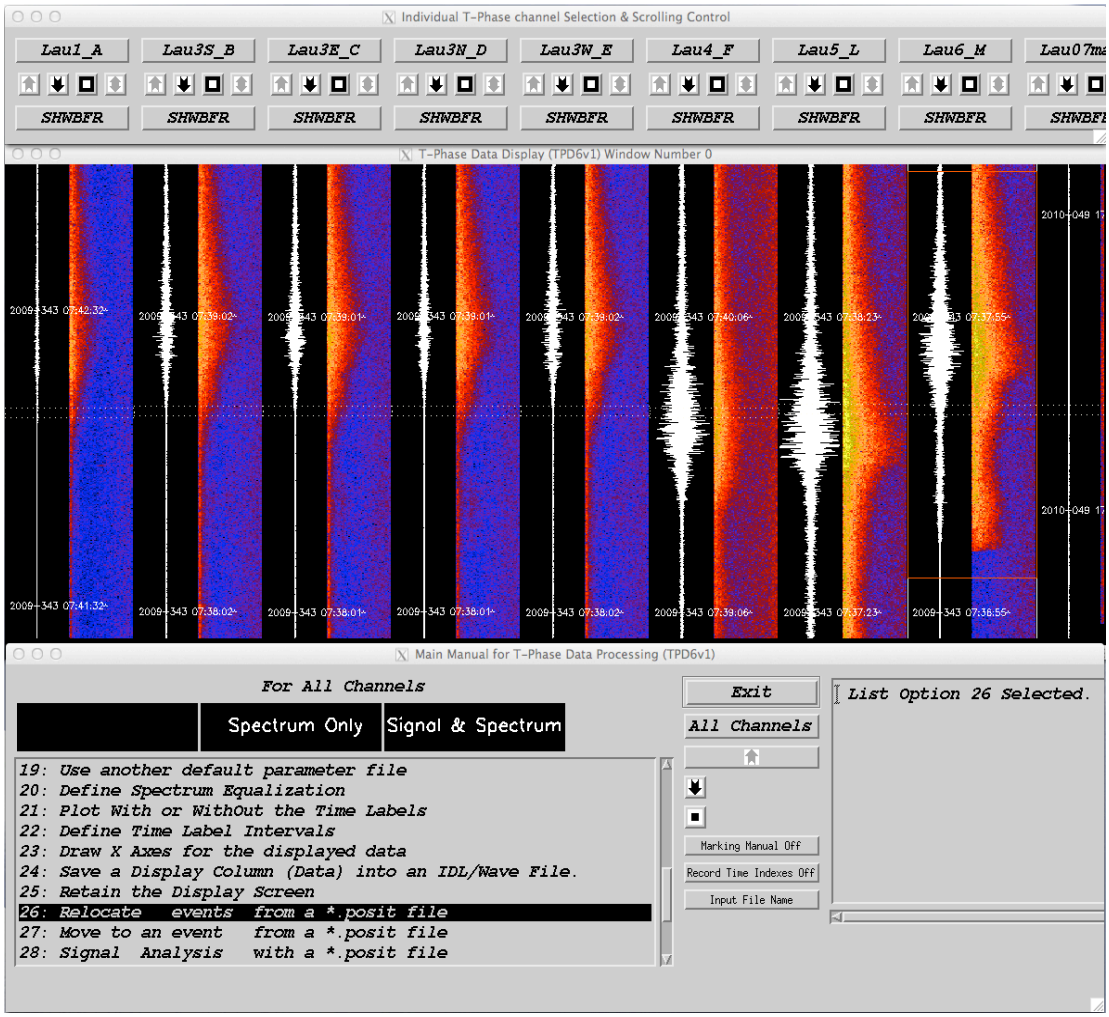

Figure 5: Seasick Hydroacoustic Processing Suite. Top panel shows hydrophone channels and corresponding signals recorded. Lower panel shows all the 28 programs available in the software package. Spectrogram shows the T-wave wave train with the highest amplitude showing point of highest acoustic energy.

3.0 RESULTS & DISCUSSION

3.0 RESULTS & DISCUSSION

The results section will examine the overall distributions of seismicity, compare seismic and T-wave location in terms of their event-pair vector differences and investigation of the relationship between acoustic source level and seismic magnitude. Figure 6 captions the overall distribution of micro seismicity along the Eastern Lau Spreading Center.

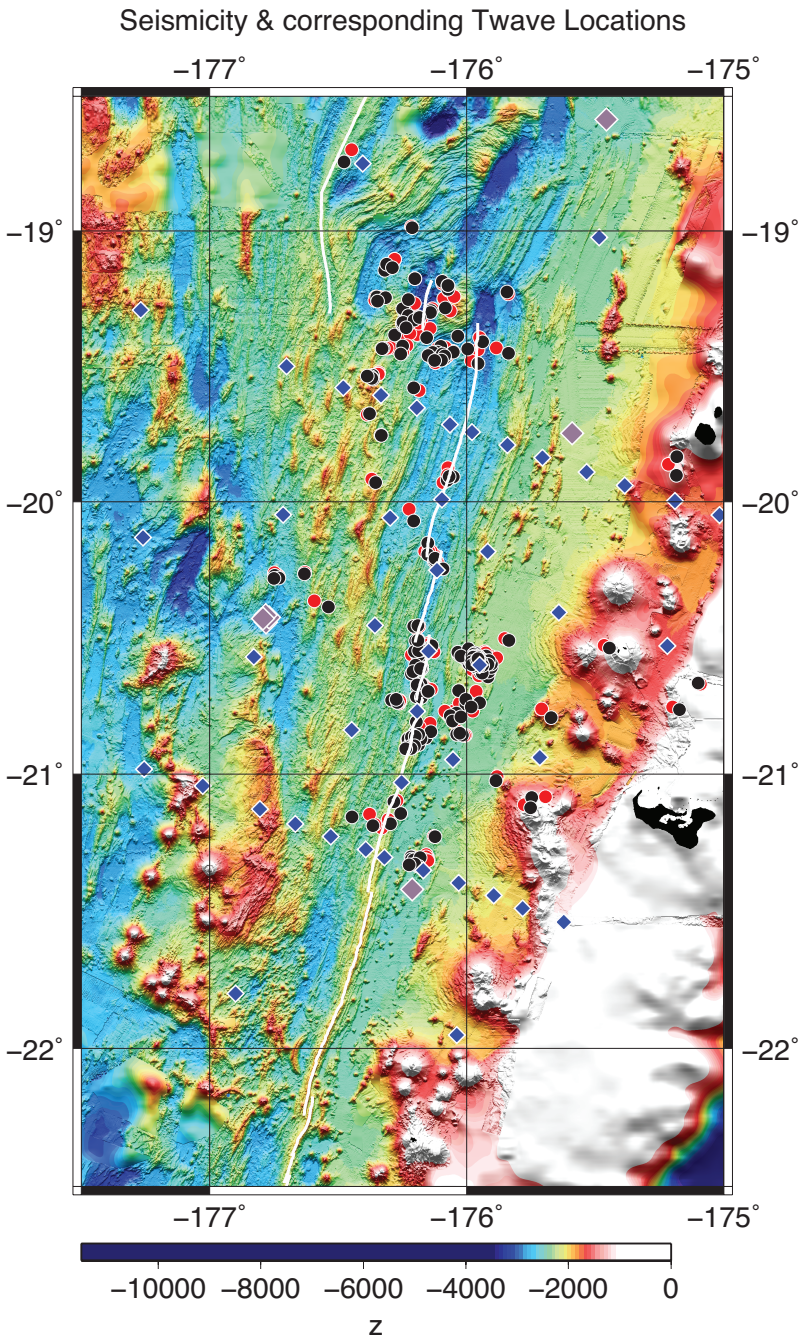

Figure 6: Bathymetric map of the Eastern Lau Spreading center (ELSC) section of the Lau Basin. The white lines show the Eastern Lau spreading center and associated second -order ridge segmentation. The blue squares show the array of 51 Ocean bottom Seismometers deployed to monitor seismicity. The purple diamonds show the location of the moored hydrophones within the SOFAR channel. The red circles indicate distribution of OBS located seismicity along the ELSC while the black circles show the T-wave located events.

3.1 OVERALL DISTRIBUTION OF SEISMICITY

Between December 2009 and April 2010, the array of 51 OBS deployed along the ELSC produced catalog of 1849 well-located local earthquakes. This catalog is limited to events with a minimum of 2 P-S phase pairs, at least 8 defining phases, and an azimuthal gap of less than 180^{o}. Approximately 5% of the events are distributed at the relay zone between the Central Lau and the Eastern Lau Spreading Centers (19^{o} 20' - 20^{o} 32' S latitude). Along the ELSC, there are five areas of concentrated earthquake activity, clusters A-E (Fig 7). Cluster A, containing ~3% of the catalog, near a small on-axis volcano that has been rifted apart by the spreading process. Further south, clusters B (~3%), C (2%) and D (11%) are located in or near a non-transform offsets in the ridge axis, with lateral offsets of 8, 4, and 1.5 km respectively. On axis near 21° 16' S latitude, cluster E contains another ~5% of the catalog. Most of the well-located earthquakes, however, lie on the eastern flank of the ELSC, approximately 45 km off axis. Cluster F contain 44% of the events and is positioned along a volcanic ridge extending to the north of an intra-plate seamount with approximately 1500 m of local relief. The longevity of activity in this area and its swarm-like evolution in time and event magnitude indicates that magmatic and possibly volcanic processes are driving the focused seismicity (Figure 8). Cluster G contain 15% of the events and is positioned along a low relief sediment-filled basin. The events are more spatially dispersed relative to cluster F. Figure 9 tracks the temporal evolution of seismicity in these areas.

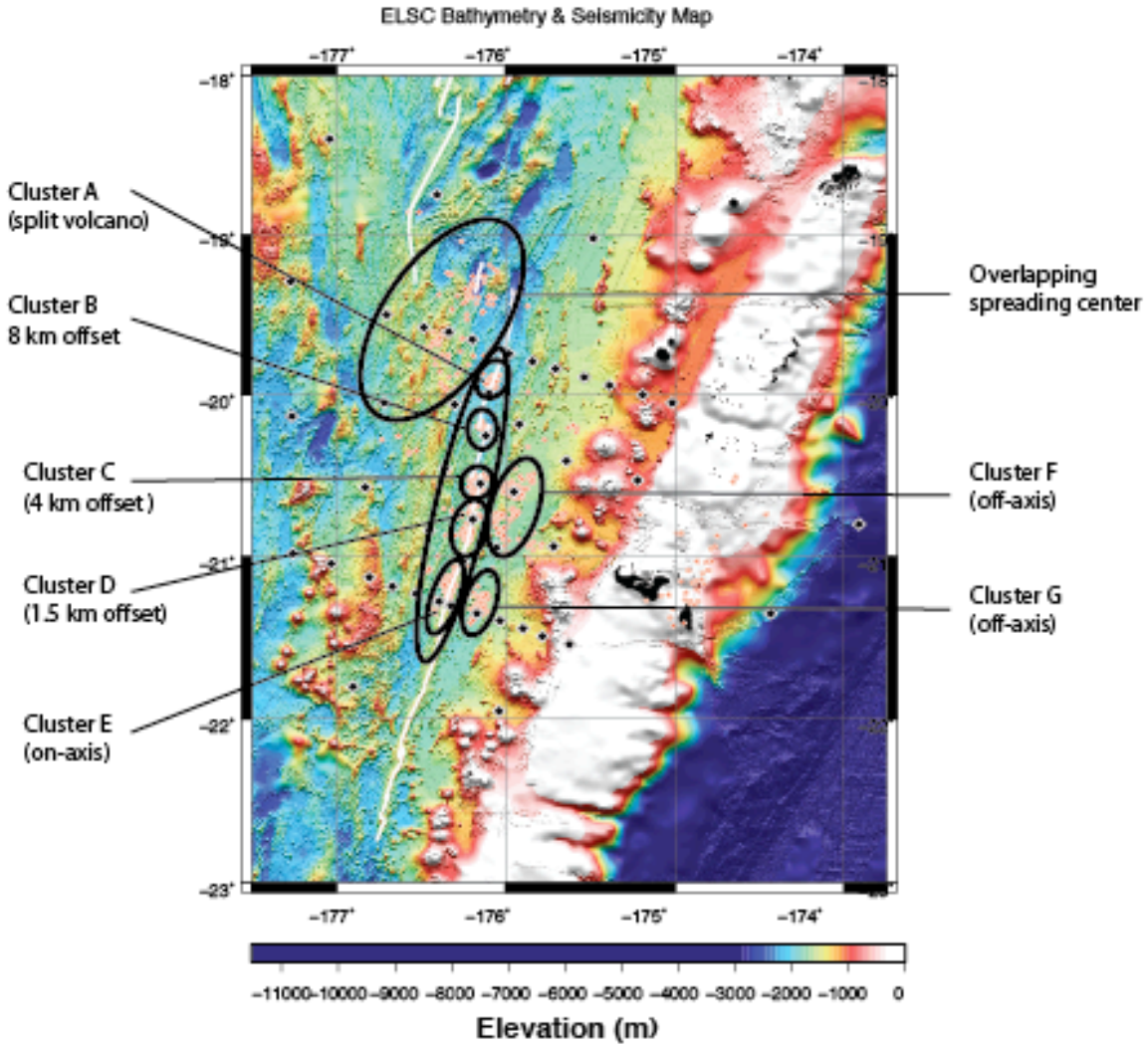

Figure 7: Bathymetric map of the Eastern Lau Spreading center (ELSC) section of the Lau Basin showing location of swarms in relation to the spreading center's morphological domains. The 8km, 4km and 1.5km lateral offsets are the widths of the overlapping centers. White line is used to outline the spreading center and the red circles indicate distribution of seismicity.

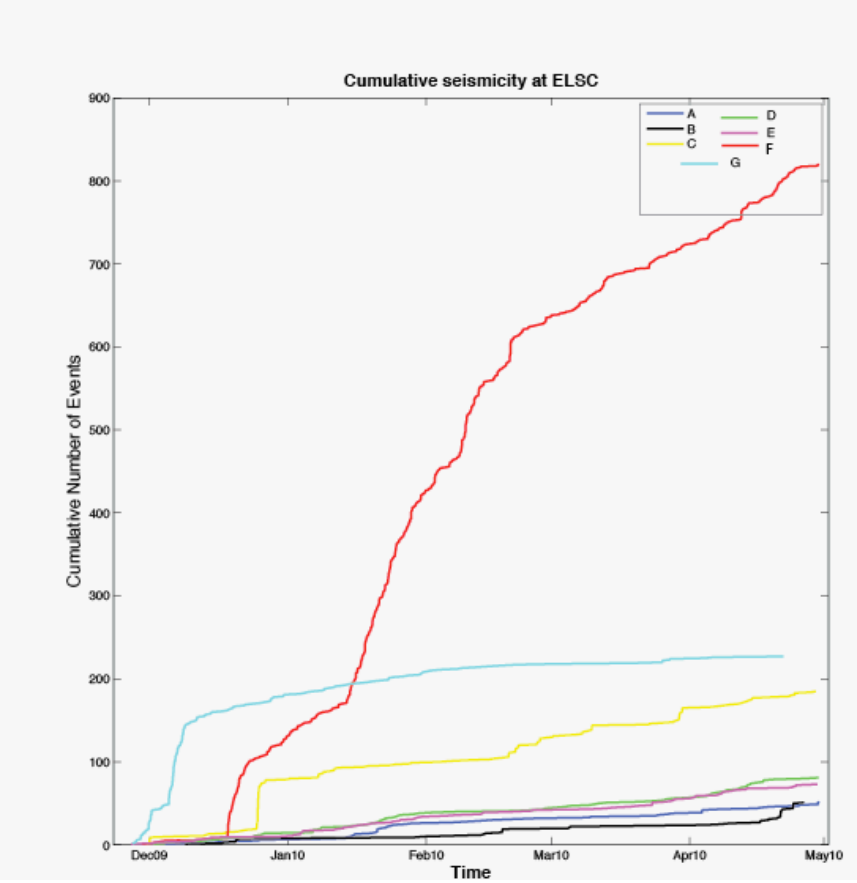

Figure. 8. Cumulative number of events along the Eastern Lau spreading center. Refer to Figure.7 for location of seismic clusters.

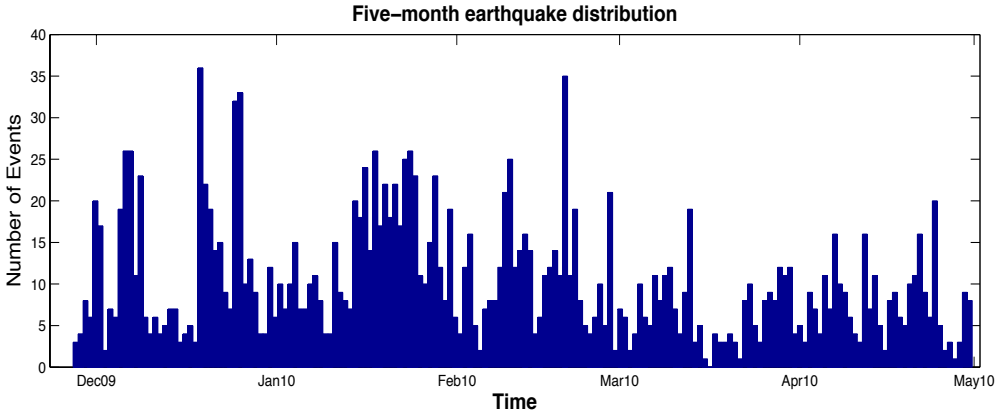

Figure. 9. Time distribution of seismicity along the Eastern Lau Spreading Center as recorded by the OBS network.

3.2 SEISMIC AND T-WAVE LOCATION COMPARISONS

Of the total of 1849 seismic events recorded during the 5-month period, only 621 (34%) of these events could be correlated with hydro-acoustically located events. The reason for this large disparity may be attributed to the positioning and different array configuration of both sensors. Ocean bottom seismometers are mounted on the seafloor 10's km apart along the Eastern Lau Spreading Center compared to the 6 autonomous underwater hydrophone station, which are moored in the SOFAR channel and separated by distances of >100 km. Note that the vertical (21.5^{o}S) and horizontal arrays (20.5^{o}S) are treated as a single station in our location analysis (Figure 5).

To make comparisons between OBS and AUH locations, a search is conducted to find the corresponding acoustic events that were generated by the earthquakes. Finding valid matches requires a trade-off between the epicentral displacement and origin time difference reported in the OBS and AUH event catalogs. From the physics of T-wave generation, a T-wave derived source location may not necessarily have the same geographic coordinates as the seismic epicenter, and even when they are co-located, the T-wave origin time should be delayed slightly by the amount of time it takes a P-wave to travel between the hypocenter and seafloor. In this study, we require that T-wave and seismic derived origin pairs must be separated by < 8 km in distance and 5.3 sec in time (which represents the time it takes for an acoustic phase to traverse laterally 8 km in the v=1.5 km/s water column) to be associated.

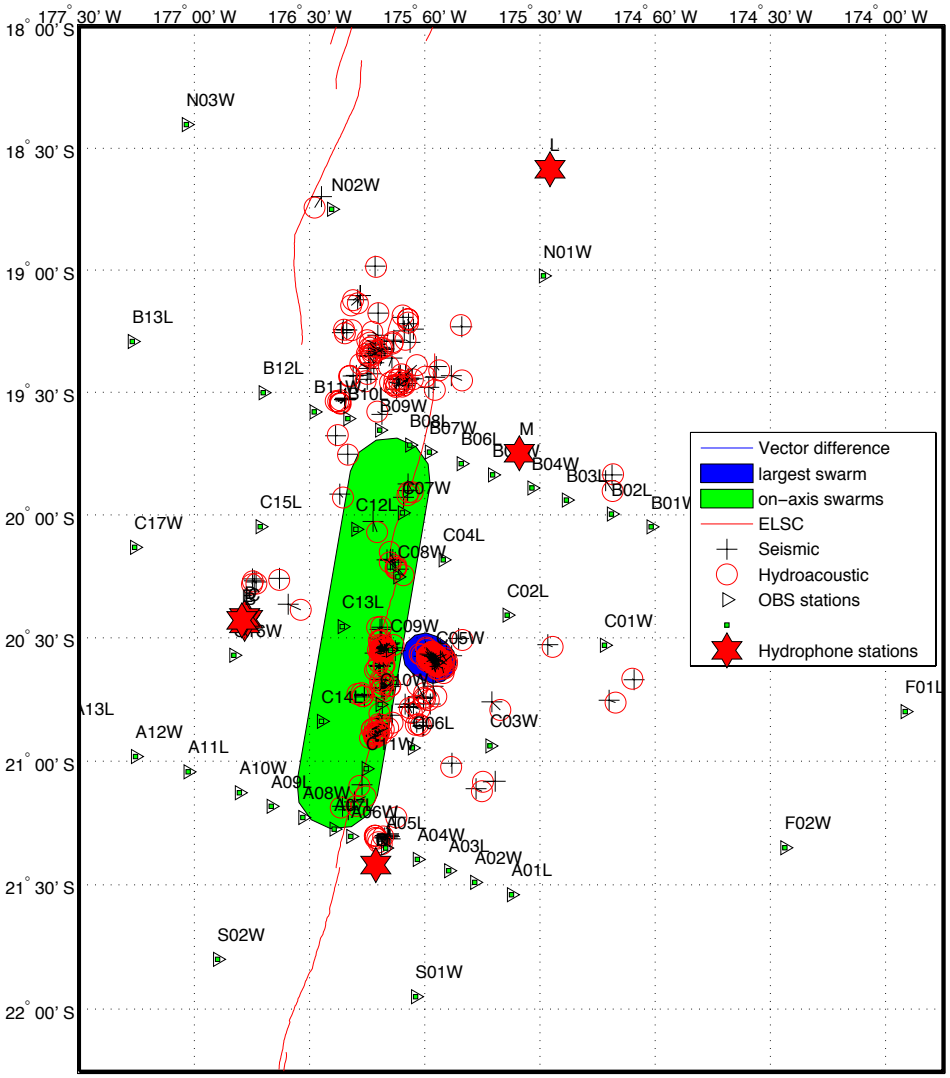

Figure. 10. Comparison of seismic and hydroacoustic locations in the Lau Basin. Solid lines drawn from OBS location (crosses) to AUH location (red circles) for 621 correlated events between November 2009 and December 2010. Only 375 events were located with more than 4 hydrophones. Along axis swarm accounts for 187 events excluding the events within the relay zone while the off-axis swarms accounts for 188 of the seismo-acoustic pairs.

The events used are restricted to those that were recorded on at least four hydrophone stations. This filtering procedure yielded a total of 375 seismo-acoustic event pairs. The 188 earthquakes that characterize the largest off-axis swarm (F, Figure 7) had a mean time delay of 2.8 sec with a standard deviation of 0.9 sec. A negative origin time difference indicates a T-wave source originating before the earthquake source—which is physically unrealistic. However, only five of these event pairs indicated an earlier T-wave origin time, all of which were > -1.0 sec. A similar evaluation was made for the swarms along the axis. The mean of the origin time differences was 3 sec with a 1.0 sec standard deviation. Only 1 of these event pairs indicated an earlier T-wave origin time, again with all values being > -1.0 second. A histogram of the origin time difference is shown in figures 11a & 11b.

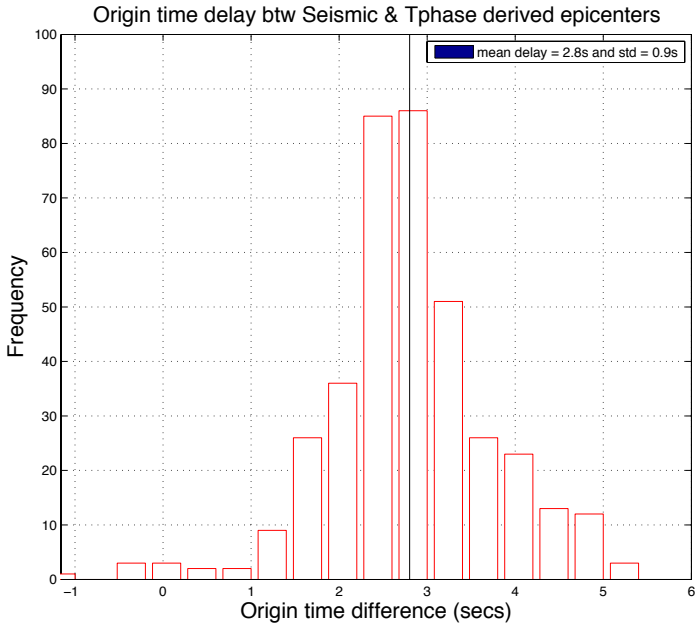

Figure.11a. Origin time differences between Seismic and T-wave locations for off-axis swarms. Origin time of OBS events is taken as a reference from which the origin times of T-wave events are subtracted from and thus the origin time difference gives positive values. Negative values indicate earlier an origin time for a T-wave located epicenter.

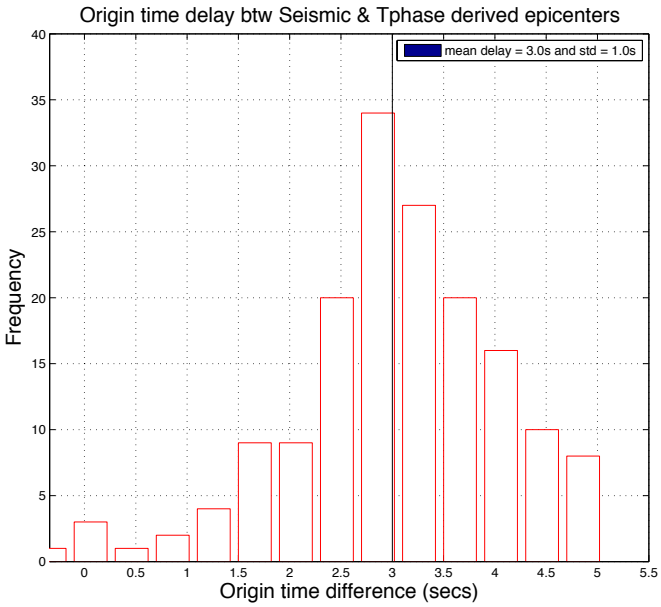

Figure.11b. Origin time differences between Seismic and T-wave locations for on-axis swarms. Origin time of OBS events is taken as a reference from which the origin times of T-wave events are subtracted from and thus the origin time difference gives positive values. Negative values indicate earlier an origin time for a T-wave located epicenter.

3.3. STATISTICAL SUMMARY OF LOCATION COMPARISON

	Q0.025 (km)	**Q25(km)**	**Q50(km)**	**Q75(km)**	**Q975(km)**	***p***	**R**	**<θ>**	**N**
OFFAXIS	0.147	0.65	1.22	2.41	5.74	0.00	0.55	164.84±9.94	185
ONAXIS	0.203	1.09	2.04	3.48	6.43	0.00	**0.34**	243.31±8.94	164

Q: percent quantile values of epicentral difference given in km
<θ>: resultant mean azimuth from AUH to OBS epicenters, _+2~ limits (circular statistic)
p: statistically random as determined by Schuster test (circular statistic, 95% confidence)
R: resultant length of circular data (circular statistic)
N: Number of events

3.3.1. AZIMUTHAL COMPARISONS

The directional bias is examined using circular statistics (Schuster, 1897), which disregards the magnitudes of the relative location vectors and considers only the azimuth between the seismic and T-wave located epicenters. For a population of N azimuths (θ1, θ2, θ3, … , θn), the mean resultant azimuth and length can be given by:

$$D^2 = \left(\sum_{i=1}^{N} \cos\theta_i \right)^2 + \left(\sum_{i=1}^{N} \sin\theta_i \right)^2 \tag{3.1}$$

where θi is the azimuth from the T-wave located epicenter to the seismic epicenter for event i. R has a range from 0 to 1 where 1 indicates that all directions are identical and values < 1.0 indicate increasing dispersion. The resultant length is a related to the circular variance as $S_0^2 = 100x\left(1-\bar{R}\right)$. The resulting p-value gives a measure of how random (p~1) or non-random (p~0) the distribution is:

$$p = \exp\left(-\frac{D^2}{N}\right) \tag{3.2}$$

Table 1 shows the circular statistics of the epicentral difference for both on-axis events and the largest off-axis swarm (F). For the off-axis swarm, the mean resultant azimuth is 164.84±9.94^o (2σ) with a length of 0.55. 75%of all the off-axis events fall within a ~2.4 km radius of the swarm center and 97.5% are within a ~6.0 km radius. Figure 12 below is a compass plot showing the azimuthal distribution of events according to epicentral difference. Schuster test from (Table 1) indicates a greater than 99% probability that the azimuths between location pairs are non-randomly distributed. Schuster test p-values obtained yielded a zero value probability.

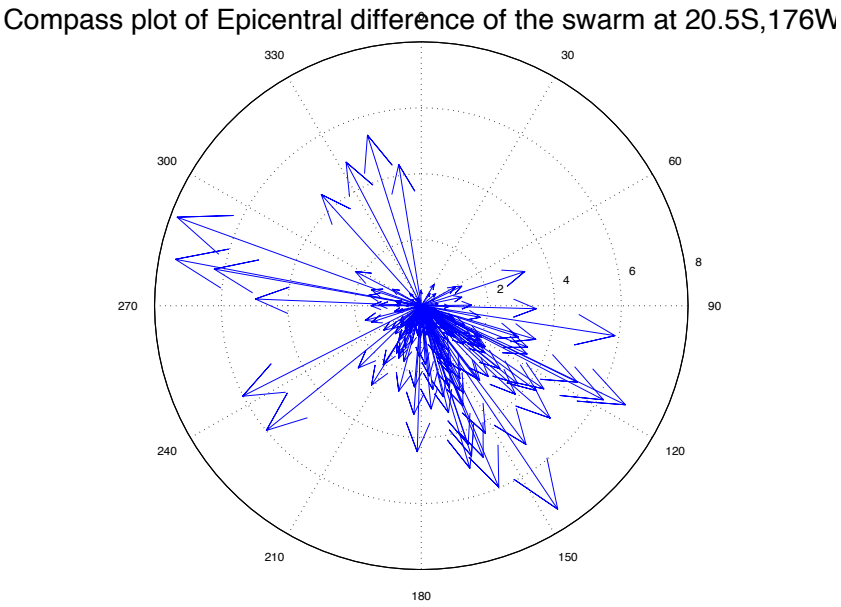

Figure.12 Compass plot of the location difference vectors between the seismic and hydroacoustically derived earthquake epicenters for the off-axis swarm. The acoustic earthquake locations are 2–6 km to the south-southeast of the seismic locations. Bathymetric steering does not seem to be a significant factor since many of the hydroacoustic earthquake locations are on a flat topography off the seamounts.

The on-axis swarms had a mean resultant azimuth of 243.31±8.94^{o} (2σ) with a length of 0.34. 75% of all the along-axis events fall within a ~3.5 km radius of the swarm center and 97.5% are within a ~6.0 km radius. Figure 13 below is a compass plot showing the azimuthal distribution of events according to epicentral difference. These along-axis hydroacoustic locations are displaced to the southwest, relative to the OBS locations. This shift in offset direction relative to the off-axis swarm reflects the geometry of the array. Schuster test p-values (Table 1) obtained also indicates a greater than 99% probability that the events are non-randomly distributed.

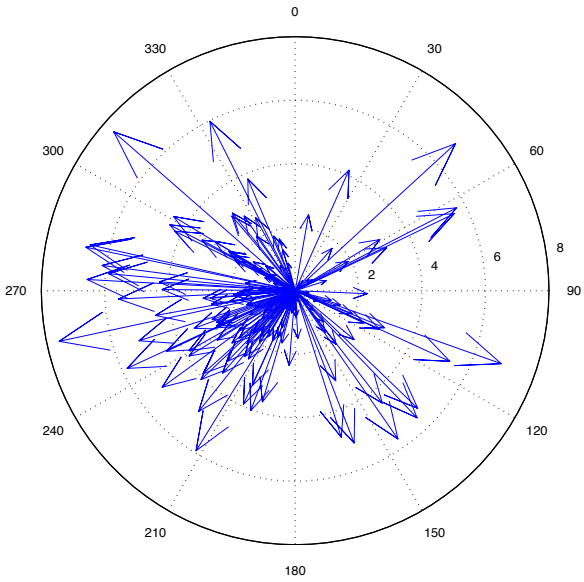

Figure.13 Compass plot of the location difference vectors between the seismic and hydroacoustically derived earthquake epicenters for the swarms along-axis. The acoustic earthquake locations are 1–5 km to the south-southwest of the seismic locations. Southwest position of quad array may play a significant role in steering many of the hydroacoustic earthquake locations towards that direction.

3.4. ERROR ANALYSIS OF SEISMO-ACOUSTIC PAIRS

The aim here is to assess the accuracy of the earthquake locations by finding how many of the T-wave derived epicenters fall within 95% confidence interval of the error ellipse associated with the seismic epicenters. The HYPOINVERSE program reports both the vertical (ERZ) and horizontal (ERH) errors, which are, simplified errors derived from the lengths and directions of the principal axes of the error ellipsoid. An error ellipsoid whose major axes are 2.4 times the standard errors calculated by HYPOINVERSE has a 95% chance of containing the "true" hypocenter. ERH is simply the length of the major axes when viewed from above and projected onto a horizontal plane.

The error ellipse provides only an estimate, though it accounts for all the geometry of the stations and ray paths. A true calculation of the error ellipse would include the uncertainties in every variable, including the crustal model, which is not feasible.

In making valid comparisons between both methods, a representative horizontal error is computed using the error in longitude and latitude reported by the hydroacoustic method. This is done by taking the larger of the errors between the longitude and latitude for each earthquake. An error ellipsoid with its major axis estimated as the standard errors calculated by the hydroacoustic software, SEASICK has a 68% chance of containing the 'true' hypocenter. Multiplying these standard errors by a factor of 1.96 gives values that represent a 95% confidence interval of the 'true hypocenter'.

Results from the error analysis of the largest off-axis swarm (F) shows that only 56.7% of the T-wave derived epicenters fall within the 95% confidence region of the seismic derived epicenters; however, for 89% of these event pairs, the 95% confidence regions (error ellipses) overlap for the seismic and hydroacoustic locations. These OBS located events tend to cluster on the dike-shape ridge extending from a large seamount (Figure 15) while T-wave events on average are located on or slightly to the south-east of this topographic feature. Notably, the T-wave location do indicate preferential coupling of sound from the peak of the seamount, which rises 1500 m above the local seafloor. The slight south-southeast shift in the T-wave epicenters may be attributed to the location of the swarm in

relation to the arrays, with two-thirds of the hydrophone stations lying to the north of the swarm area.

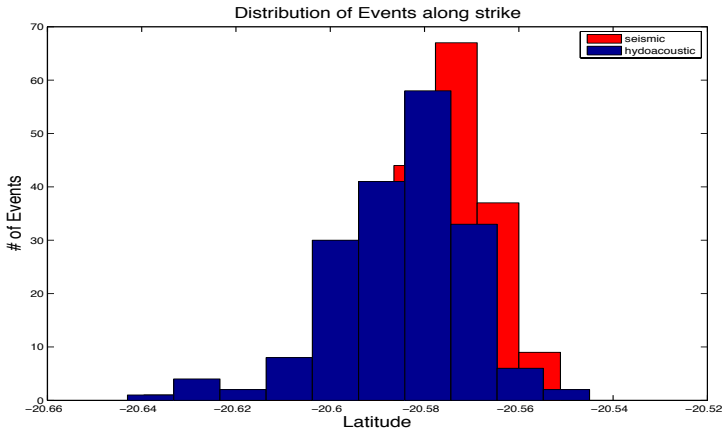

Figure.14. Distribution of earthquakes off-axis at 20.5^{o} along strike. Blue histogram represents hydroacoustic events while red histogram represents seismic events.

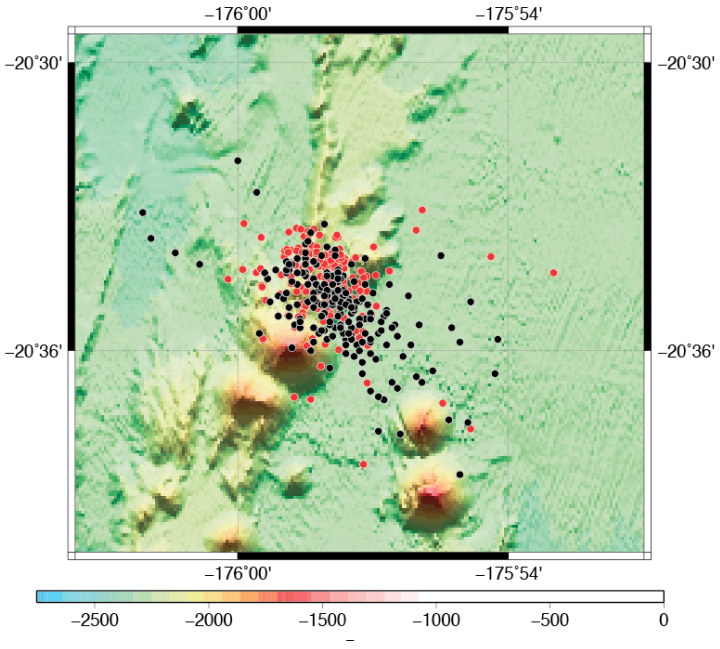

Figure.15. Bathymetric map showing location of OBS and Hydrophone located epicenters. Black dots represent T-wave source locations and Red dots represent seismic epicenters. The two seamounts southwest of the swarm do not contribute to bathymetric steering.

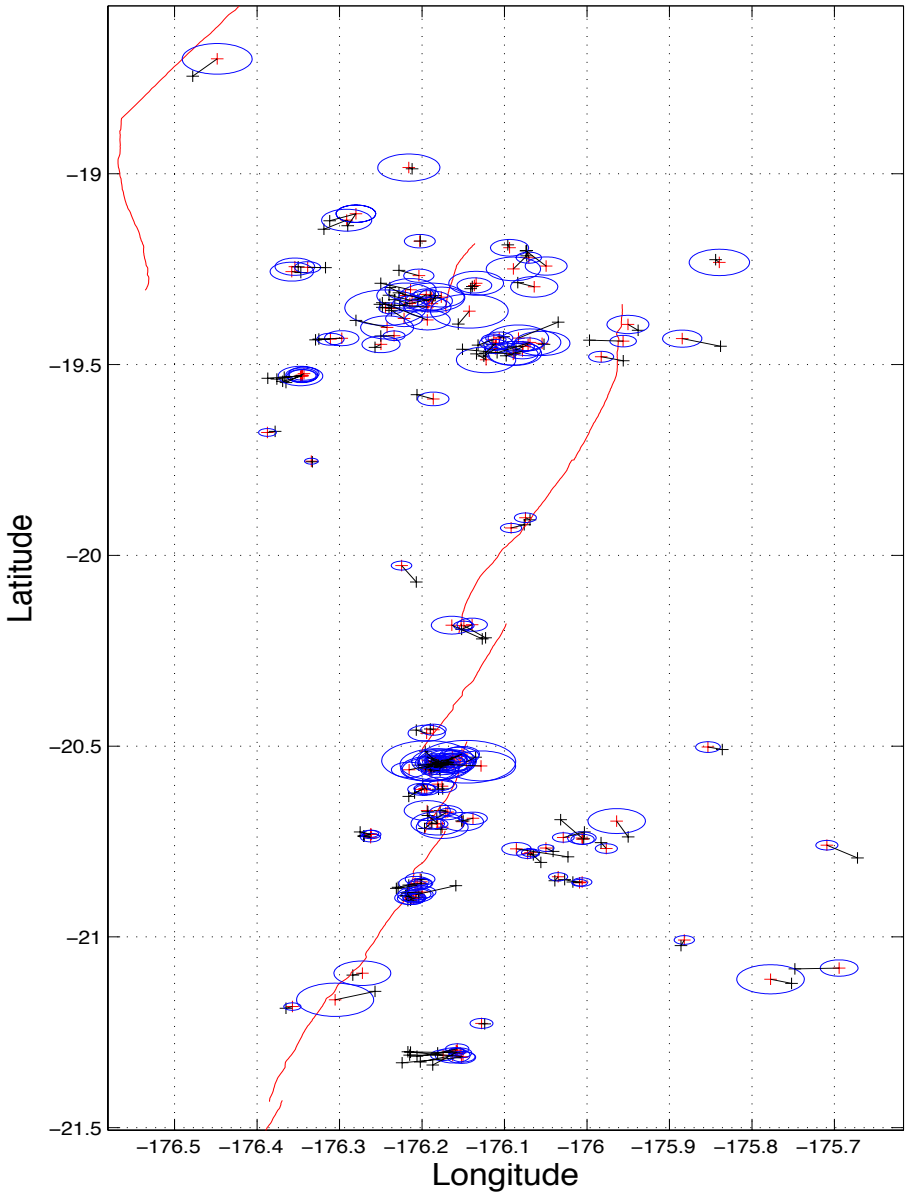

Figure.16. Error estimates for the off-axis events along the spreading axis at 95% confidence interval. The black lines show the vector difference between seismo-acoustic pairs of events. Black crosses represent the T-wave events while the red crosses indicate the seismic events.

Also, our study shows that 46.4% of the T-wave epicenters along the axis fall within the 95% confidence region of the seismic derived epicenters; however, for 87% of these event pairs the 95% confidence regions (error ellipses) overlap for the seismic and hydroacoustic locations (Figures 18).

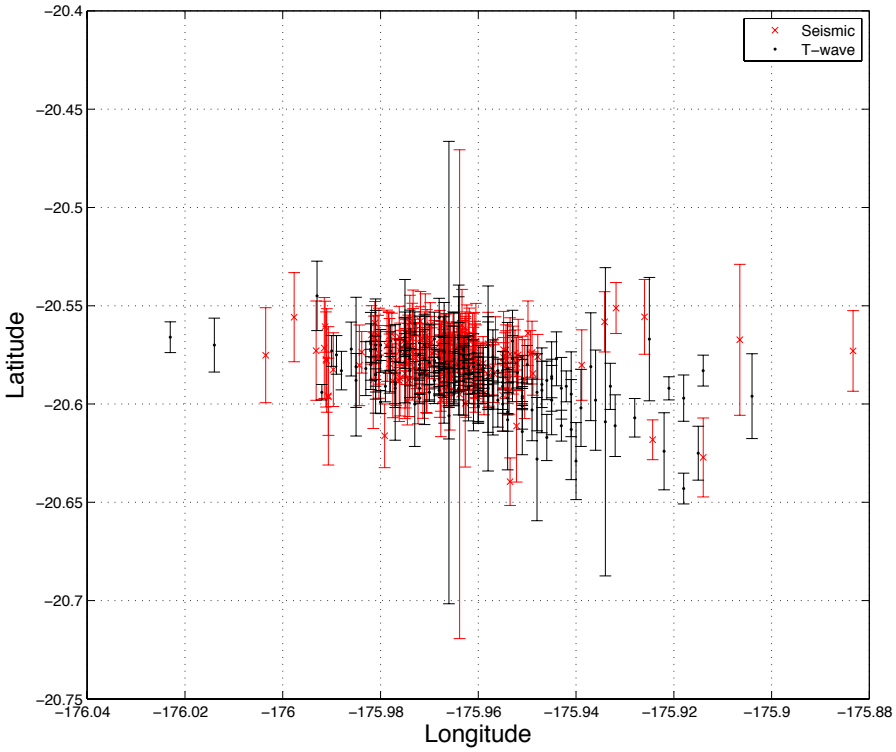

Figure.17. Horizontal errors for both the seismic and hydroacoustic locations of the off-axis swarm at 20.5^{o}. A total of 183 pairs of events are represented with error bars depicting 95% confidence interval of the 'true hypocenter'. Blue error bars denote T-wave events and Black error bars denote seismic events.

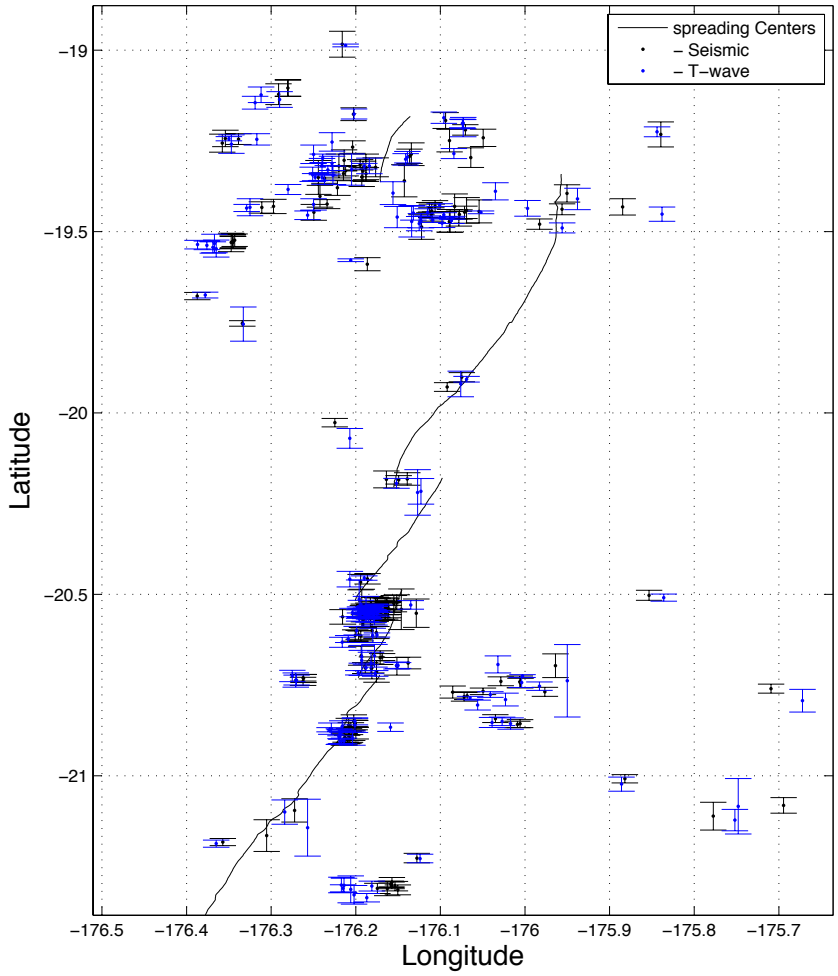

Figure.18. Horizontal errors for both the seismic and hydroacoustic locations along the Eastern Lau spreading Center. A total of 187 pairs of events are represented with error bars depicting 95% confidence interval of the 'true hypocenter'. Blue error bars denote T-wave events and Black error bars denote seismic events.

For the off-axis swarm at 20.5° S, the mean 95% uncertainty in the OBS–derived locations obtained using HYPOINVERSE is 1.77 km, with a two-sigma range of 1.67 km to 2.03 km (Figure 18). The mean 95% uncertainty in the hydrophone–derived locations obtained using

SEASICK is 1.47 km, with a two-sigma range of 1.32 km to 1.72 km (Figure 18). There is no significant difference in the predicted accuracy of events located on or off-axis. The reported location accuracy for T-wave sources is consistent with Monte Carlo simulation for the error field within the larger aperture equatorial Pacific region based on a method, which posits an accuracy of <4km at 95% confidence level Fox.et al. (2001).

Table 3 summarizes the location differences observed for event pairs. Smaller mean differences in location and origin time are observed for the off-axis swarm compared to the on-axis swarms. It is important to note that individual swarms along the axis have a low sample population, thus we have combined multiple swarms from different regions of the axis. Slightly higher differences on axis may be as a result of the topographic variations, with many of the axis events lying with a broad axial valley that is somewhat shallower than the off-axis swarm site. This is in line with Williams' et al. (2006) prediction of weaker T-waves at deeper seafloor depths thus increasing the uncertainty of picking the peak amplitude of a T-wave arrival.

Table 3. 2. Descriptive statistics of earthquake parameters. Bootstrap technique is used since parameters do not follow a normal distribution.

	OFF-AXIS		ON-AXIS	
	Mean	**Std**	**Mean**	**Std**
Epicentral difference (km)	1.73±0.21	1.65	2.45±0.26	1.82
Time difference (secs)	2.63±0.08	0.56	3.03±0.15	1.03
Magnitude	1.72±0.05	0.35	1.8±0.07	0.45
Depth (km)	2.87±0.52	7.65	0.44±0.33	7.46

3.5. RELATIONSHIP BETWEEN EARTHQUAKE SOURCE PARAMETERS AND EPICENTRAL DIFFERENCE

3.5.1 ACOUSTIC SOURCE LEVEL VS SEISMIC MAGNITUDE

These results allow for contemporaneous study of low-level seismicity recorded on both the OBS and hydrophone arrays. The acoustic source level (SL) of a T-wave is regarded as the overall contribution from the received level of the signal and transmission loss between the source and the receiver. Acoustic source levels within the off-axis swarm range from 179.4 – 220 dB re 1 mPa @ 1 m while along the axis range between 184.26 - 228 dB re 1 mPa @ 1 m (Figures 19 & 20). Local earthquake magnitudes range from 1.0-2.8 ML along the axis and 0.8-3.3 ML with the off-axis swarm near 20.5° S.

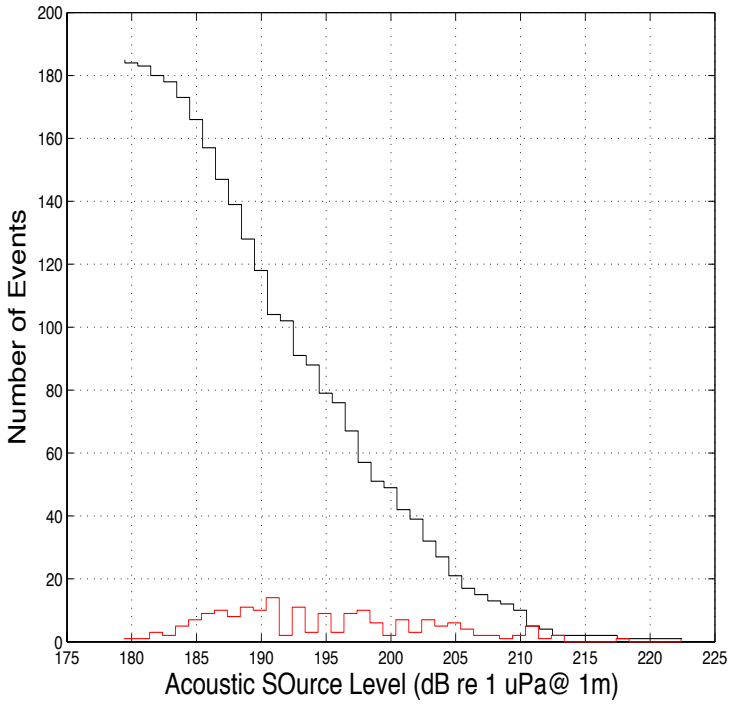

Figure. 19 Histograms of T wave acoustic source levels for the off-axis swarm at 20.5° S recorded in the Lau basin for the period Nov 2009 to Apr 2010. Only events recorded on four or more hydrophones were included. The lower (red) histogram shows the number of events per 1-dB class interval and indicates that detections are consistent across the whole range of source levels. The cumulative histogram shown above illustrates the importance of seismic sources to the ambient noise field of the ocean, with about 120 events in the swarm having source levels of 190 dB or greater

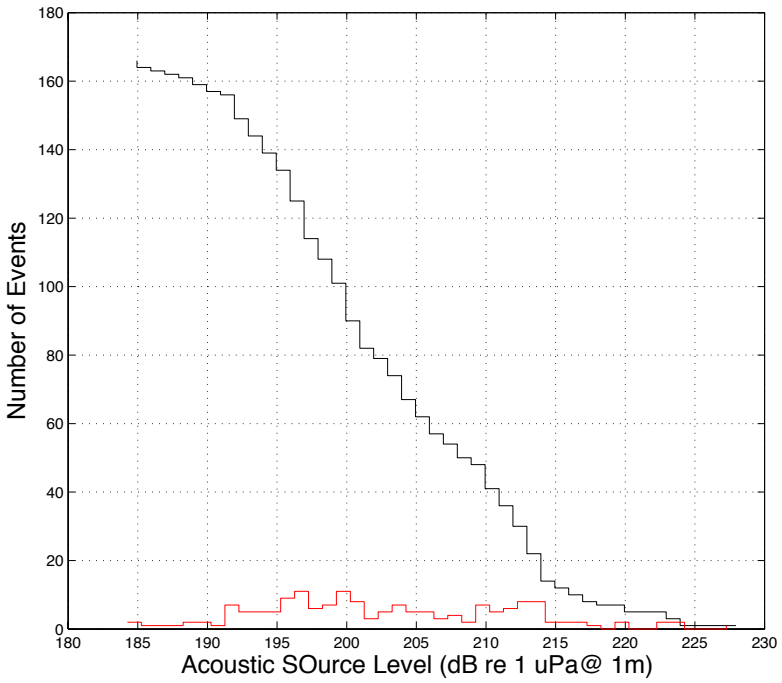

Figure. 20 Histograms of T wave acoustic source levels for the along-axis swarms recorded in the Lau basin for the period Nov 2009 to Apr 2010. Only events recorded on four or more hydrophones were included. The lower (red) histogram shows the number of events per 1-dB class interval and indicates that detections are consistent across the whole range. The cumulative histogram shown above illustrates the importance of seismic sources to the ambient noise field of the ocean, with about 152 out of the 162 events in the swarm with 190 dB or greater

A positive correlation exists between acoustic source levels and seismic magnitudes (Figures 21 & 22). Previous results have confirmed a linear relationship for events with common focal mechanism, propagation path (e.g., Pulli and Upton, 2002; Yang and Forsyth, 2003). Dziak (2001) reported empirical relationships between the acoustic source level and the seismic magnitude showing that T-wave energy release in the ocean water column is lower for normal and reverse fault earthquakes than strike slip events. For the off-axis swarm

at 20.5° S, coefficient of determination from the regression analysis yields a R^2 value of 0.46 ± 0.05, with a slope of 15.77±1.32 and intercept of 170.22±2.32. The regression analysis of the along-axis swarms yields a R^2 value of 0.59 ± 0.04, with a slope of 14.97±0.98 and intercept of 175.47±1.82. Although focal mechanism solutions do not exist for these small earthquakes, based on seafloor faulting patterns, extensional (normal faulting) earthquakes along N-NE trending planes are expected to dominate both off and on axis. This result suggests that the strength of the correlation and regression coefficients are influenced by either small (unresolved) differences in the depths of these events [e.g., Yang and Forsyth, 2003; Slack et al. 1999] or efficiency of propagation between the source and receiver [e.g., Bohnenstiehl, D. R., Scheip, C. M., Matsumoto, H., & Dziak, R. P. (2012). Acoustic variability of air gun signals recorded at intermediate ranges within the Lau Basin. *Geochemistry Geophysics Geosystems*, *13*, doi:10.1029/2012GC004337]. Notably, propagation paths are similar for the tightly clustered events within the swarm at 20.5° S and they exhibit a slightly weaker correlation thus suggesting variable depths (or potentially variable focal mechanisms) within the swarm, which we have interpreted to be of magmatic origin.

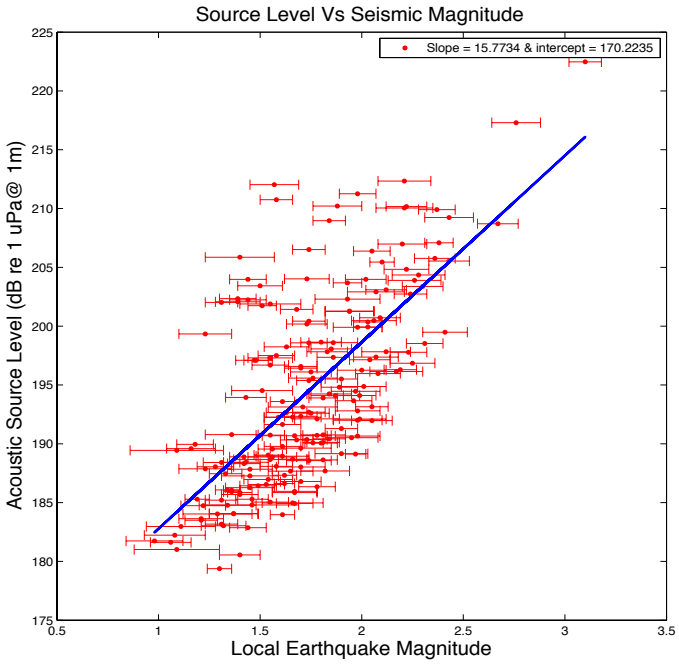

Figure 21. Observed relationship between acoustic source level and corresponding seismic magnitude reported in Lau basin earthquake catalog. The regression analysis is limited to the off-axis swarm (183 events) in the catalog. The prediction equation ASL = 15.77 ML + 170 (where ASL is acoustic source level in dB). The results are highly significant with R^2 = 0.461.

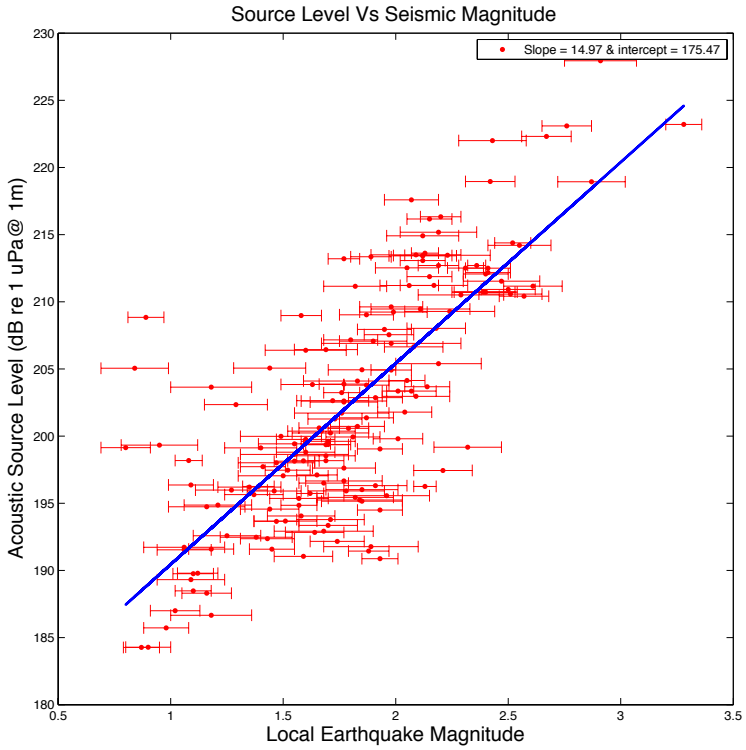

Figure 22. Observed relationship between acoustic source level and corresponding seismic magnitude reported in Lau basin earthquake catalog for the along-axis swarms (164 events). The prediction equation ASL = 14.97 ML + 175.47 (where ASL is acoustic source level in dB). The results are highly significant with $R^2 = 0.592$.

3.5.2 EPICENTRAL DIFFERENCE VS NO. OF HYDROPHONE STATIONS

The epicentral difference with respect to number of stations is explored by computing probability density histograms thus allowing for base comparison as the histogram is normalized and therefore will integrate to one. To eliminate the many confounding factors associated with variable propagation paths, this relationship is investigated for the off-axis swarm at 20.5° S only. T-wave arrival times recorded on at least three hydrophone stations were used for this analysis, and a total of 6 hydrophone stations were deployed over the duration of the project. Comparing mean epicentral difference estimates (Table.4) across all hydrophones reveals a median location offset of less than or equal to 2 km.

Since the location differences are not normally distributed, a non-parametric Mann-Whitley test was conducted to test the null hypothesis that the data are from populations with equal medians. The result **p** is the probability of observing the given result, or one more extreme, by chance if the null hypothesis (that the medians are equal) is true at 5% significant level. Small values of **p** (e.g., < 0.05) would therefore cast doubt on the validity of the null hypothesis; however, our results ($p > 0.2$) indicate that we can reject the null hypothesis that the medians are equal (Figure 24).

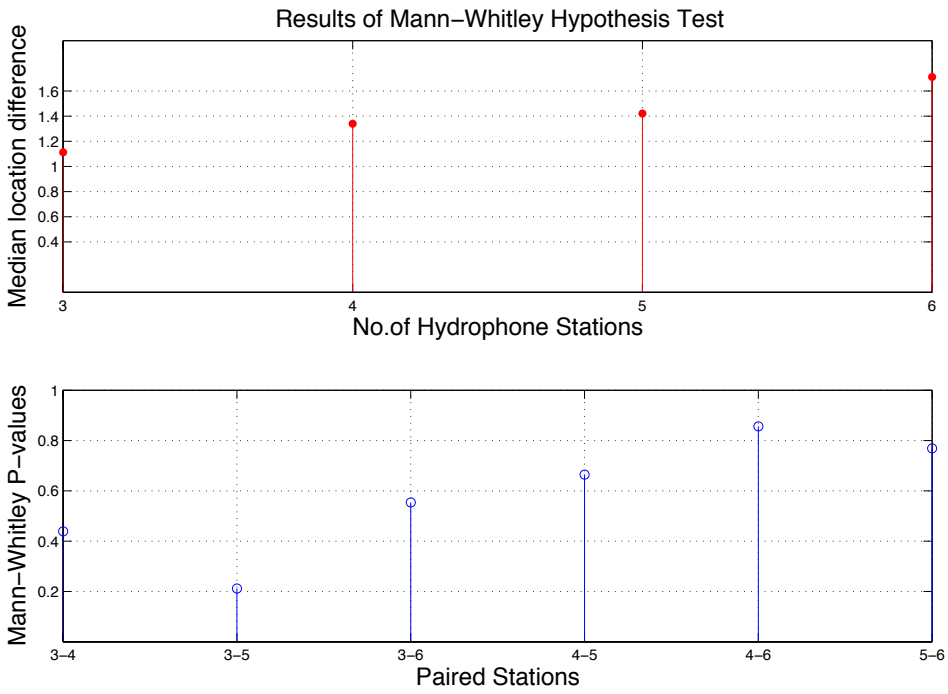

Figure. 23. Figures showing the results of Mann-Whitley test. Above shows that events located with indicated number of hydrophones have significantly different medians at 5% significance level. Below shows the p-values for each pair of hydrophone stations compared. All paired tests

Generally it should be the case that increasing the number of T-wave arrivals used in the location would improve the accuracy of the result and therefore result in a smaller location difference; however, here we find that there is no significant trend in terms of location difference and number of hydrophone stations used. We suggest that larger earthquakes also produce longer duration T-wave arrival packets, which may lead to great uncertainty in the arrival times used in locating these events.

Table 4. Statistics of epicentral difference recorded with number of hydrophone stations for the largest off-axis swarm at 20.5° S (swarm F). N represents the number of events located. Q: percent quantile values of epicentral difference given in km.

Number of Stations	3 (N = 98)	4 (N = 44)	5 (N = 28)	6 (N = 13)
Mean epicentral difference (km)	1.53±0.25	1.89±0.50	2.04±0.6	2.00±0.88
Median epicentral difference (km)	1.12±0.26	1.34±0.57	1.42±0.59	1.72±1.15
Quantiles				
Q25	0.62	0.61	0.78	0.55
Q75	2.03	2.64	2.89	2.96
Q97.5	4.91	6.14	6.13	5.25

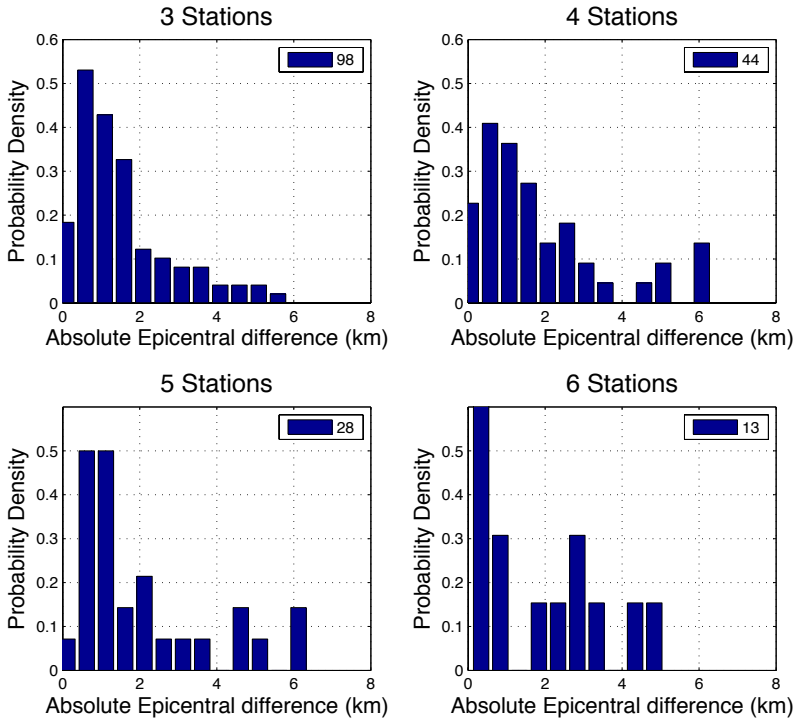

Figure. 24. Probability density distribution of epicentral difference between seismo-acoustic pairs with respect to the number of stations used in the location. Bin width 0.5 km.

4.0 SUMMARY & CONCLUSION

1. We have compared the seismic and hydroacoustic derived locations of earthquakes in the Lau basin to resolve location accuracies reported by these two methods. Out of the 1849 earthquakes that were located using the OBS array, 375 of these events could be correlated with earthquakes within the T-wave derived catalog. The detection of significantly more events by the OBS array reflects the much greater density of OBS vs. AUH stations along the ELSC. The overall pattern of seismicity, as viewed through both datasets, is similar, with earthquakes clustered along the axis and on the eastern flank of the ELSC.

2. Along the spreading axis, 46.4% of the T-wave located events fall within the 95% confidence interval for the corresponding OBS derived location, with the confidence ellipses overlapping for 89% of the origin pairs. Approximately 56.7% of the T-wave located events within the largest off-axis swarm (near 20.5° S) fall within the 95% confidence interval for the corresponding OBS derived location, with the confidence ellipses overlapping for 87% of the origin pairs. For these events, the location differences between AUH and OBS catalogs show no dependence on the number of hydrophone stations used in the solution. Based on these findings, we infer that there are no significant differences in the location accuracy between the dense 51-station OBS and spare 6-station AUH arrays deployed within the basin. Moreover, we find no evidence that T-waves locations are biased by topography within the Lau Basin.

3. A positive correlation exists between acoustic source levels and local seismic magnitudes. For the off-axis swarm at 20.5° S, the best fitting linear regression has a slope of 15.77±1.32 and intercept of 170.22±2.32, and for the along-axis data we find a slope of 14.97±0.98 and intercept of 175.47±1.82. Regression coefficients indicated that approximately 59% (R^2=0.59 ± 0.05) and 46% (R^2=0.46 ± 0.04) of the variance in acoustic source level could be explained by magnitude for the off-axis and along-axis populations, respectively. Additional variability is related to some combination of propagation effects and differences in the depth or faulting mechanism of the earthquakes.

FUTURE RECOMMENDATIONS

The earthquake locations obtained in this study could be improved using waveform cross-correlation. This method utilizes the fact that an ensemble of data from a region of the earth observed at a single station will have very similar waveforms. This is because wave propagation in the earth is the primary factor that converts a relatively simple source pulse into a long string of pulses to make up seismic data. Sources at nearly the same point or nearly the same space will excite similar propagation modes and therefore record similar time series data. This has not been extensively utilized in T-wave applications.

REFERENCES

Barry R. Lienert Assessment of earthquake location accuracy and confidence region estimates using known nuclear tests *Bulletin of the Seismological Society of America, October 1997, v. 87, p. 1150-1157*

Boyd, T. M. and Snoke, J. A., 1984, Error Estimates in some Commonly Used Earthquake Location Programs, *Earthquake Notes* **55**, 3–6.

Bohnenstiehl, D.R., R. P. Dziak, H. Matsumoto, J. Conder, Acoustic response of submarine volcanoes in the Tofua Arc and northern Lau Basin to two great earthquakes, GJI, 2014

Bohnenstiehl, D. R., Scheip, C. M., Matsumoto, H., & Dziak, R. P. (2012). Acoustic variability of air gun signals recorded at intermediate ranges within the Lau Basin. *Geochemistry Geophysics Geosystems*, *13*, doi:10.1029/2012GC004337.

Bohnenstiehl, D.R. and M. Tolstoy, Comparison of Teleseismic- and Hydroacoustic-Derived Earthquake Locations along the North-Central Mid-Atlantic Ridge and Equatorial East-Pacific Rise, SRL, 74(6) SRL 790-801, 2003

Bormann, P. (2012 online): Magnitude calibration formulas and tables, comments on their use and complementary data. - In: Bormann, P. (Ed.), *New Manual of Seismological Observatory Practice 2 (NMSOP-2)*, Potsdam : Deutsches GeoForschungsZentrum GFZ, p. 1-19. DOI: http://doi.org/10.2312/GFZ.NMSOP-2_DS_3.1

Bradley, C. R., and R. A. Stephen (1996), Modeling of seafloor wave propagation and acoustic scattering in 3□D heterogeneous media, J. Acoust. Soc. Am., 100, 225-236, doi:10.1121/1.415952.

Brian Taylor, Kirsten Zellmer, Fernando Martinez, Andrew Goodliffe, Sea-floor spreading in the Lau back-arc basin, Earth and Planetary Science Letters, Volume 144, Issues 1–2, October 1996, Pages 35-40, ISSN 0012-821X, http://dx.doi.org/10.1016/0012-821X(96)00148-3.

Brodie, D., and R. Dunn (2011), Detection of baleen whales on an ocean-bottom seismometer array in the Lau Basin, Abstract S31D-2266 presented at 2011 Fall Meeting, AGU, San Francisco, Calif., 5–9 Dec.

Collins, J. A., D. K. Smith, *and* J. J. McGuire *(*2012*),* Seismicity of the Atlantis Massif detachment fault, 30°N at the Mid-Atlantic Ridge*,* Geochem. Geophys. Geosyst.*,* 13*,* *Q0AG11,*

Colosi, J. *(*2004*),* Theory of long-range acoustic propagation*, paper presented at* Seismo-acoustic Applications in Marine Geology and Geophysics Workshop*, Appl. Phys. Lab., Univ. of Wash., Woods Hole Oceanogr. Inst.,* Woods Hole, Mass.

Conder, J. A., and D. A. Wiens (2011), Shallow seismicity and tectonics of the central and northern Lau Basin, Earth and Planet. Sci. Lett., 304, 538-546, doi:10.1016/j.epsl.2011.02.032.

de Groot-Hedlin, C. D., and J. Orcutt (1999), Synthesis of earthquake□generated T□waves, Geophys. Res. Lett., 26(9), 1227-1230, doi:10.1029/1999GL900205.

de Groot-Hedlin, C., and J. Orcutt (2001), Excitation of T-waves by seafloor scattering, J. Acoust. Soc. Am., 109, 1944-1954, doi:10.1121/1.1361057, doi:10.1121/1.1361057.

Dunn R.A., Martinez F. Contrasting crustal production and rapid mantle transitions beneath back-arc ridges*. Nature* 2010*;*46*:*198-202*.*

Dunn R.A., Martinez F., Conder J.A. Crustal construction and magma chamber properties along the Eastern Lau Spreading Center*. Earth planet. Sci. Lett.* 2013*;*371–372*:*112-124*.*

Dziak, R. P.*,* C. G. Fox*, and* A. E. Schreiner *(*1995*),* The June-July 1993 seismo-acoustic event at CoAxial segment, Juan de Fuca Ridge: Evidence of lateral dike injection*,* Geophys. Res. Lett.*,* 22*,* 135–138*.*

Dziak, R.P., 1997, Acoustic monitoring of earthquakes along the Blanco transform fault zone and Gorda Pl. and their tectonic implications: Oregon State University, unpublished Ph.D. dissertation, 187

Dziak, R. P. *(*2001*),* Empirical relationship of T-wave energy and fault parameters of northeast Pacific Ocean earthquakes*,* Geophys. Res. Lett.*,* 28*,* 2537–2540*.*

Dziak, R. P.*,* D. K. Smith*,* D. R. Bohnenstiehl*,* C. G. Fox*,* D. Desbruyeres*,* H. Matsumoto*,* M. Tolstoy*, and* D. J. Fornari *(*2004*),* Evidence of a recent magma dike intrusion at the slow spreading Lucky Strike segment, Mid-Atlantic Ridge*,* J. Geophys. Res.*,* 109*, B12102, doi:10.1029/2004JB003141*.*

Ewing, W. M., and J. L. Worzel (1948), Long-range sound transmission, Geolog. Soc. Am., Mem. 27, 1-35.

Fox, C. G.*,* H. Matsumoto*, and* T.-K. A. Lau *(*2001*),* Monitoring Pacific Ocean seismicity from an autonomous hydrophone array*,* J. Geophys. Res.*,* 106*(*B3*),* 4183–4206

Gary L. Pavlis Appraising earthquake hypocenter location errors: A complete, practical approach for single-event locations *Bulletin of the Seismological Society of America December 1986 76:1699-1717*

H. Matsumoto; D.R. Bohnenstiehl; R.P. Dziak; L. Williams; R. Gliege; C.N. Meinig; P. Harben, (2010), A vertical hydrophone array coupled via inductive modem for detecting deep-ocean seismic and volcanic sources MTS/IEEE Seattle, OCEANS 2010

Husen, S., and J.L. Hardebeck (2010), Earthquake location accuracy, Community Online Resource for Statistical Seismicity Analysis, doi:10.5078/corssa-55815573

Johnson, R. H., R. A. Norris, and F. K. Duennebier (1968), Abysally generated T-waves, in The Crust and Upper Mantle of the Pacific Area, Geophys. Monogr. Ser., vol. 12, edited by L. Knopoff, C. L. Drake, and P. J. Hart, pp. 70–78, AGU, Washington, D. C.

Kayal, J. R. 2008. Microearthquake seismology and seismotectonics of South Asia. New Delhi: Capital Pub. Co.

Klein, F. W.*,* Hypocenter location program HYPOINVERSE*,* U.S. Geol. Surv. Open File Rep*78-694,* 2012.

Norris, R. A.*, and* R. H. Johnson *(*1969*),* Submarine volcanic eruptions recently located in the Pacific by Sofar hydrophones*,* J. Geophys. Res.*,* 74*,* 650–664

Pan, J.*, and* A. M. Dziewonski *(*2005*),* Comparison of mid-oceanic earthquake epicentral differences of travel time, centroid locations, and those determined by autonomous underwater hydrophone arrays*,* J. Geophys. Res.*,* 110*, B07302*

Park, M., R. I. Odom, and D. J. Soukup (2001), Modal scattering: A key to understanding oceanic T□waves, Geophys. Res. Lett., 28(17), 3401-3404, doi:10.1029/2001GL013472.

Pulli, J. J.*, and* Z. M. Upton *(*2002*),* Hydroacoustic observations of Indian earthquake provide new data on T-waves*,* Eos Trans. AGU*,* 83*, p.* 145.

Slack, P.D., C.G. Fox, and R.P. Dziak. 1999. P-wave detection thresholds, Pn velocity estimates, and T wave location uncertainty from oceanic hydrophones. *Journal of Geophysical Research* 104:13,061–13,072

Schuster, A. *(*1897*),* On lunar and solar periodicities of earthquakes*,* Proc. R. Soc. London*,* 61*,* 455–465.

Tolstoy, M. and D.R. Bohnenstiehl, Hydroacoustic contributions to understanding the

December 26th 2004 great Sumatra–Andaman Earthquake, Sur. Geophys. DOI 10.1007/s10712-006-9003-6, 2006

Tolstoy, I., and M. Ewing (1950), The T phase of shallow-focus earthquakes, Bull. of the Seismol. Soc. Am., 40(1), 25-51.

Urick, R., D. Heiberg and J. Davis (Eds.) (1983), Principles of Underwater Sound, McGraw-Hill, New York, NY.

Williams, C. M., R. A. Stephen, and D. K. Smith (2006), Hydroacoustically recorded seismicity at the intersection of the Atlantis (30N) and Kane (23 40′N) Transform Faults with the Mid-Atlantic Ridge, Geochem. Geophys. Geosyst.7, Q06015

Yang, Y., *and* D. W. Forsyth *(*2003*),* Improving epicentral and magnitude estimation of earthquakes from T phases by considering the excitation function*,* Bull. Seismol. Soc. Am.*,* 93*,* 2106–2122

Zellmer, K. E.*, and* B. Taylor *(*2001*),* A three-plate kinematic model for Lau Basin opening*,* Geochem. Geophys. Geosyst.*,* 2*(5), 1020*

APPENDICES

APPENDIX 1 - PROGRAM TO FIND VALID SEISMO-ACOUSTIC PAIRS OF EVENTS.

```
%% 1. Read in all Seismic Data

% OBS data
load hyp_catalogs_jubrilMS_withML; % Magnitudes
%load('OBS_hypoinversedata.mat');
%load magYL.mat;% magnitudes

% HYDROPHONE data
tarr = rdhydrophone('hydarrivals'); % arrivals
t = rdhydroevent('hydlocfile'); % origin


%% 2. Set up Time Vector

% setup OBS time vector
hypo.time = [hypo.yr,hypo.mo,hypo.da,hypo.hr,hypo.mn,hypo.sc];
% Now convert to serial date number
hypo.time = datenum(hypo.time);

% set Hydrophone time vector
mon= zeros(size(t.yr));day = zeros(size((t.yr)));
for i = 1:length(t.jd)
[mon(i) day(i)] = jd2monday(t.yr(i),t.jd(i));
t.mo(i) = mon(i); t.da(i) = day(i);
end
t.time = [t.yr,t.mo',t.da',t.hr,t.min,t.sc];

% Now convert to serial date number
t.time = datenum(t.time);

%% 3. Find events common to OBS and Hydrophone using Origin time

% Initialize array
time_delay = zeros(size(t.time,1), size(hypo.time,1));

min_time_delay = zeros(size(t.time));indx = zeros(size(t.time));
for i = 1:length(t.time);

    % subtract origin times from OBS and AUH
    time_delay(i,:) = abs(bsxfun(@minus,t.time(i),hypo.time));
    %raw_origin_diff(i,:) = bsxfun(@minus,t.time(i),hypo.time);

    % get only minimum values from the matrix
    min_time_delay(i) = transpose(min(time_delay(i,:)))*86400;
% in seconds

    % Not considering the absolute values - just the raw differences
    %raw_min_time_delay(i) = transpose(min(raw_time_delay(i,:)))*86400;

    % get the index values of the origin times in hypo catalog
    indx(i) = find(time_delay(i,:) == min(time_delay(i,:)));

    % get indices for the raw time delay
```

```
    %raw_indx(i) = find(raw_time_delay(i,:) == min(raw_time_delay(i,:)));
end

%% 5. Visualize Histogram distribution of time delay (TOTAL = 610 EVENTS)
figure(1);
bin = min(min_time_delay):20:max(min_time_delay);
[freq,bin]=hist(min_time_delay,bin);
bar(bin,freq);
h = findobj(gca,'Type','patch');
set(h,'Facecolor','w','Edgecolor','r');
xlabel('Origin time delay in btw OBS and Hydrophone (secs)','fontsize',16)
ylabel('Frequency','fontsize',16)
title('Distribution of Origin time delay btw OBS & AUH','fontsize',16)

% Define catalog for events common to OBS
HYPO = keeprowsarray(hypo,indx'); %

save('~/Documents/Research/OBS611.mat','HYPO');
%% 7. Visualize difference in origin times on a Comb plot

                        %=========FIGURE 2========
figure(2);
stem(t.time,min_time_delay)
axis([min(t.time) max(t.time) 0 300])
xlabel('Hydrophone origin time','fontsize',14);
dateformat = 12;
datetick('x',dateformat,'keeplimits')
ylabel('Min Origin time diff relative to OBS (secs)','fontsize',14);
title('Stem plot showing minimum origin time delay btw OBS &
AUH','fontsize',16);

%% 8. Compute Vector Difference between points and plot vector

[arclen,az] = (distance(HYPO.lat,HYPO.lon,t.lat,t.lon));
distkm = deg2km(arclen);
tmp_matrix =zeros(size(HYPO.lat,1),2);
tmp_matrix = [distkm az];% arc length and azimuthal difference between AUH
& OBS
km_indx = find(distkm);

%% 9. Find valid OBS & AUH events using Epicentral difference & expected
time delay

% Compute expected time delay within crust
tcrust = 8/5; %distance/p velocity;
% Within water column
twater = 8/1.5; %distance/velocity of sound in water
tdelay = tcrust + twater

%% DEFINE THE 381 VALID SUBSET BASED ON OBS & AUH EVENTS
% 9a. Crietria - distkm <= 8 & min_time_delay <= 5.33
%=========================================================
subset = find(distkm <= 6.9 & min_time_delay <= 5.33);
```

```
n8 = length(subset)
% define new catalog of events based on an accuracy of less than 8km in
lat &  lon
HYPO = keeprowsarray(HYPO,subset);
t = keeprowsarray(t,subset);

%% 9b. Plot basin-wide Magnitude vs Source Level
whitebg
figure(3);
plot(HYPO.ML, t.SL,'.r');hold on
xlabel('Local Earthquake Magnitude')
ylabel('Acoustic Source Level')
title('Source Level Vs Seismic Magnitude')
coeff = polyfit(HYPO.ML,t.SL,1);
pred_SL = polyval(coeff,HYPO.ML,1);
plot(HYPO.ML,pred_SL,'b')
legend('ML vs SL','Slope = 15.7734 & intercept = 170.2235','Northeast')

%% 9c. Statistics
% Calculate mean and standard deviation of the difference in origin time
tdelay = (t.time - HYPO.time)*86400;
med_tdelay = median(tdelay)
mean_tdelay = mean(tdelay)
std_tdelay = std(tdelay)

figure;
stem(HYPO.time,tdelay)


% Compute Quantiles
Q = quantile(tdelay,[0.25,0.5,0.75]);
Q25 = Q(1)
lessQ25 = length(find(tdelay <= Q25))
Q50 = Q(2)
lessQ50 = length(find(tdelay <= Q50))
Q75 = Q(3)
lesQ75 = length(find(tdelay <= Q75))

% HISTOGRAM OF THE TIME DELAY FOR VALID OBS & AUH MATCHES
whitebg('w')
figure(4);
bin = min(tdelay):0.4:max(tdelay);
[freq,bin]=hist(tdelay,bin);
bar(bin,freq);hold on
grid on;
xm = [2.8,2.8];ym =[0,120];
plot(xm,ym,'k')
axis([min(tdelay) 6 0 100])
h = findobj(gca,'Type','patch');
set(h,'Facecolor','w','Edgecolor','r');
xlabel('Origin time difference (secs)','fontsize',16)
ylabel('Frequency','fontsize',16)
title('Origin time delay btw Seismic & Tphase derived
epicenters','fontsize',16)
```

```
legend('mean delay = 2.8s and std = 0.9s', 'Location','Northeast');

%% THESE ARE THE VALID 381 OBS & AUH LOCATED EARTHQUAKE PAIRS

%==== Save this new OBS & AUH catalog to a Matlab file=====
% === subset with distkm <= 8 & min_time_delay <= 5.33=====
save('~/Documents/Research/matlabscripts/validOBS.mat','HYPO');
save('~/Documents/Research//matlabscripts/validAUH.mat','t');

%% Plot minimum distance and minimum time delay=========

dist_sub = distkm(subset);
figure(5);
stem(dist_sub,tdelay,'LineStyle','-','MarkerFaceColor','red',...
     'MarkerEdgeColor','k')
%axis([min(dist_sub) max(dist_sub) 0 max(tdelay)])
xlabel('Epicentral Difference','fontsize',14);
ylabel('time delay','fontsize',14);
title('Stem plot showing Epicentral difference vs time
delay','fontsize',16);

% Dot Plot of Epicentral Distance & Time delay
figure(6);
whitebg;
siz = 8:8:40
gscatter(dist_sub,tdelay,t.nsta,'crymg','.',siz);hold on
plot(dist_sub,tdelay,'.k')
grid on
xlabel('Absolute Epicentral difference (km)','fontsize',14)
ylabel('Time delay(secs)','fontsize',14)
title('Epicentral difference vs Time delay with distkm<10 &
timedelay<6','fontsize',16);

% Dot Plot of Epicentral Distance & Time delay for events less than 2secs
figure(7);
whitebg('w'); a = dist_sub<2;
epi_less2 = dist_sub(a);
plot(epi_less2, tdelay(a),'.r')
xlabel('Epicentral difference in km','fontsize',14);
ylabel('Time delay(secs)','fontsize',14);
title('Epicentral difference less than 2km vs Time delay','fontsize',16);

%% 10. Plot Epicentral Map of OBS and AUH based on subset 1
figure(8);
%a. define projection first
axesm('MapProjection','Mercator');
setm(gca,'MapLatLimit',[-22.25 -18],'MapLonLimit',[-177.5 -173.75])
lat = [-20.595;-20.57]; lon = [-175.96; -176.0];
plotm(lat,lon);hold on
%% b1. Create buffer around largest swarm
[lat_buffer,lon_buffer] = bufferm(lat,lon,0.09); % buffer defined with
0.07 degree arc length
geoshow(lat_buffer,lon_buffer, 'DisplayType','polygon','facecolor','blue')
```

```
%c. get cordinates of events within the polygon
H_in = inpolygon(HYPO.lat,HYPO.lon,lat_buffer,lon_buffer);
T_in = inpolygon(t.lat,t.lon,lat_buffer,lon_buffer);
H_out = find(H_in==0);
T_out = find(T_in==0);
%d. Subset the events with the largest swarm and write to file
dykOBS = keeprowsarray(HYPO,H_in);
dykHYD = keeprowsarray(t,T_in);
axisOBS = keeprowsarray(HYPO,H_out);
axisHYD = keeprowsarray(t,T_out);
save('~/Documents/Research/matlabscripts/dikeOBS.mat','dykOBS');
save('~/Documents/Research/matlabscripts/dikeHYD.mat','dykHYD');
save('~/Documents/Research/matlabscripts/axis_OBS.mat','axisOBS');
save('~/Documents/Research/matlabscripts/axis_HYD.mat','axisHYD');

%% b2. Create buffer around along-axis swarms
lataxis = [-21.41;-19.85]; lonaxis = [-176.38; -176.15];
[lat_axisbuffer,lon_axisbuffer] = bufferm(lataxis,lonaxis,0.225); % buffer
defined with 0.07 degree arc length
geoshow(lat_axisbuffer,lon_axisbuffer,
'DisplayType','polygon','facecolor','green')

%c. get cordinates of events within the polygon
Ha_in = inpolygon(HYPO.lat,HYPO.lon,lat_axisbuffer,lon_axisbuffer);
Ta_in = inpolygon(t.lat,t.lon,lat_axisbuffer,lon_axisbuffer);
Ha_out = find(Ha_in==0);
Ta_out = find(Ta_in==0);
%d. Subset the events with the largest swarm and write to file
onaxisOBS = keeprowsarray(HYPO,Ha_out);
onaxisHYD = keeprowsarray(t,Ta_out);
save('~/Documents/Research/matlabscripts/onaxis_OBS.mat','onaxisOBS');
save('~/Documents/Research/matlabscripts/onaxis_HYD.mat','onaxisHYD');
%%

%====================================
%f. Load coordinates for spreading axes & Plot
Axxis = load('~/Documents/MATLAB/rd_antelope/d_misc/neovolcanic.xyz');

%e. plot your earthquake data
plotm(Axxis(:,2),-(360-Axxis(:,1)),'r');hold on
plotm(HYPO.lat,HYPO.lon,'k+','Markersize',8,'Linewidth',0.1);hold on
plotm(t.lat,t.lon,'ro','Markersize',8,'Linewidth',0.1);

%g. Load OBS stations
fd = fopen('~/Documents/MATLAB/rd_antelope/d_misc/obs_stations.txt','r');
stats = textscan(fd,'%f %f %d %s %s\n');
plotm(stats{2},stats{1},'k>','Markersize',7)
%h. Plot the vector between both catalogs
for i = 1: length(subset);
    plotm([HYPO.lat(i),t.lat(i)],[HYPO.lon(i),t.lon(i)],'-k');
end
%i. Insert legends
legend('Vector difference','largest swarm','along
axis','Seismic','Hydroacoustic','Location','Best')
```

```
%j. Set axes properties
setm(gca,'Frame','on','grid','on','LabelUnits','dm')
setm(gca,'ParallelLabel','on','MeridianLabel','on');
setm(gca,'MLabelLocation',0.5,'PLabelLocation',0.5);
setm(gca,'MLineLocation',0.5,'PLineLocation',0.5)
gridm on
tightmap
```

APPENDIX 2 – PROGRAM TO INVESTIGATE INFLUENCE OF EARTHQUAKE PARAMETERS ON EPICENTRAL DIFFERENCE

```
%% 1. LOAD BOTH OBS & AUH DATA

% load the volcanic swarm at 20.50
load dikeOBS.mat; % seismic events
load dikeHYD.mat; % Acoustic events

filter = find(dykHYD.nsta > 5);
dykHYD = keeprowsarray(dykHYD,filter);
dykOBS = keeprowsarray(dykOBS,filter);
aa = strmatch('NW',dykHYD.comm) % events not in window
dykHYD = delrowsarray(dykHYD,aa)
dykOBS = delrowsarray(dykOBS,aa)

%% 2. EPICENTRAL displacement with number of STATIONS
% % Calculate epicentral difference
 [epi_diff,az] = distance(dykOBS.lat,dykOBS.lon,dykHYD.lat,dykHYD.lon);
 epi_diff = deg2km(epi_diff);
%
 tdelay = sort(abs(dykOBS.time - dykHYD.time))*86400;
%
% % Events With 5 hydrophones
% n5 = find(dykHYD.nsta == 5);length(n5)
% HYD_5sta = dykHYD.nsta(n5); epi_diff5 = epi_diff(n5);

%% Epicentral difference vs number of stations follows histogram
distribution
%*******************************************************
% Events With 6 hydrophones
figure;
n6 = find(dykHYD.nsta == 6);length(n6)
HYD_6sta = dykHYD.nsta(n6); epi_diff6 = epi_diff(n6);
%Now plot the Histograms
subplot(2,2,1);
%get binwidths
b = min(epi_diff6):0.5:max(epi_diff6);
%plot as density histogram
[freq,bin]=hist(epi_diff6,b); % get frequency & bin centers
area = 0.5*sum(freq);
Nden = freq/area;
bar(bin,Nden)
axis([0 8 0.0 0.6])
xlabel('Absolute Epicentral difference (km)','fontsize',14)
ylabel('Probability Density','fontsize',14)
```

```
title('3 Stations','fontsize',16)
%% Estimate the mean & std of the epidiff with 6stations
mean6 = mean(bootstrp(10000,@mean,epi_diff6))
conmeanBCA6=bootci(10000,{@mean,epi_diff6},'alpha',0.05,'type','bca') %
BCA confidence limits

median6 = mean(bootstrp(10000,@median,epi_diff6))
stderror6 = std(bootstrp(10000,@median,epi_diff6)) % standard error
confmedianBCA6=bootci(10000,{@median,epi_diff6},'alpha',0.05,'type','bca')
% BCA confidence limits
Q6 = quantile(epi_diff6,[0.025,0.25,0.5,0.75,0.975])
sumNden6 = sum(Nden)*0.5
totalEV = sum(freq)
legend(num2str(totalEV),'Location','NorthEast')
grid on
%%
%*******************************************************
% Events With 7 hydrophones
n7 = find(dykHYD.nsta == 7);length(n7)
HYD_7sta = dykHYD.nsta(n7); epi_diff7 = epi_diff(n7);
subplot(2,2,2);
b = min(epi_diff7):0.5:max(epi_diff7);
[freq,bin]=hist(epi_diff7,b);
area = 0.5*sum(freq);
Nden = freq/area;
bar(bin,Nden)
axis([0 8 0.0 0.6])
xlabel('Absolute Epicentral difference (km)','fontsize',14)
ylabel('Probability Density','fontsize',14)
title('4 Stations','fontsize',16)
%%
mean7  = mean(bootstrp(10000,@mean,epi_diff7))
median7 = mean(bootstrp(10000,@median,epi_diff7))
confmeanBCA7=bootci(10000,{@mean,epi_diff7},'alpha',0.05,'type','bca') %
BCA confidence limits

stderror7 = std(bootstrp(100000,@median,epi_diff7)) % standard error
confmedianBCA7=bootci(10000,{@median,epi_diff7},'alpha',0.05,'type','bca')
% BCA confidence limits
Q7 = quantile(epi_diff7,[0.025,0.25,0.5,0.75,0.975])
totalEV = sum(freq)
legend(num2str(totalEV),'Location','NorthEast')
grid on
%%
%*******************************************************
% Events With 8 hydrophones
n8 = find(dykHYD.nsta == 8);length(n8)
AUH_8sta = dykHYD.nsta(n8); epi_diff8 = epi_diff(n8)
subplot(2,2,3);
b = min(epi_diff8):0.5:max(epi_diff8);
[freq,bin]=hist(epi_diff8,b);
area = 0.5*sum(freq);
Nden = freq/area;
bar(bin,Nden)
```

```
axis([0 8 0.0 0.6])
xlabel('Absolute Epicentral difference (km)','fontsize',14)
ylabel('Probability Density','fontsize',14)
title('5 Stations','fontsize',16)
%%
mean8  = mean(bootstrp(10000,@mean,epi_diff8))
confmeanBCA8=bootci(10000,{@mean,epi_diff8},'alpha',0.05,'type','bca') %
BCA confidence limits

median8 = mean(bootstrp(10000,@median,epi_diff8))
stderror8 = std(bootstrp(10000,@median,epi_diff8)) % standard error
confmedianBCA8=bootci(10000,{@median,epi_diff8},'alpha',0.05,'type','bca')
% BCA confidence limits
Q8 = quantile(epi_diff8,[0.025,0.25,0.5,0.75,0.975])
totalEV = sum(freq)
legend(num2str(totalEV),'Location','NorthEast')
grid on
%%
%*******************************************************

% Events With 9 hydrophones
n9 = find(dykHYD.nsta == 9);length(n9)
HYD_9sta = dykHYD.nsta(n9); epi_diff9 = epi_diff(n9);
subplot(2,2,4);
b = min(epi_diff9):0.5:max(epi_diff9);
[freq,bin]=hist(epi_diff9,b);
area = 0.5*sum(freq);
Nden = freq/area;
bar(bin,Nden)
axis([0 8 0.0 0.6])
xlabel('Absolute Epicentral difference (km)','fontsize',14)
ylabel('Probability Density','fontsize',14)
title('6 Stations','fontsize',16)

%% Calculate standard error and 95% confidence limits on the median using
the nonparametric bootstrap method in Matlab.
% Note that by default Matlab reports bias corrected percentile
% (BCA) confidence limits; these are more accurate than those
% obtained using the standard percentile method.
mean9  = mean(bootstrp(10000,@mean,epi_diff9))
confmeanBCA9=bootci(10000,{@mean,epi_diff9},'alpha',0.05,'type','bca') %
BCA confidence limits
median9 = mean(bootstrp(10000,@median,epi_diff9))
stderror9 = std(bootstrp(10000,@std,epi_diff9)) % standard error
confmedianBCA9=bootci(10000,{@median,epi_diff9},'alpha',0.05,'type','bca')
% BCA confidence limits
Q9 = quantile(epi_diff9,[0.025,0.25,0.5,0.75,0.975])
totalEV = sum(freq)
legend(num2str(totalEV),'Location','NorthEast')
grid on

%% TEST FOR SIGNIFICANTLY DIFFERENT MEDIANS
[p1,h1,stats1]=ranksum(epi_diff6,epi_diff7)
[p2,h2,stats2]=ranksum(epi_diff6,epi_diff8)
```

```
[p3,h3,stats3]=ranksum(epi_diff6,epi_diff9)
[p4,h4,stats4]=ranksum(epi_diff7,epi_diff9)
[p5,h5,stats5]=ranksum(epi_diff8,epi_diff9)

figure;
nstats = [3,4,5,6];meanloc = [median6,median7,median8,median9];
plot(nstats,meanloc,'.r','MarkerSize',16)
grid on
xlabel('No.of Stations','fontsize',16)
ylabel('Median location difference','fontsize',16)
```

APPENDIX 3 - %% STATISCAL ANALYSI OF OFF-AXIS SWARMS -THE DIKE INTRUSIVE EVENT AT 20.5

```
%% load origin data
load 'dikeOBS.mat';
load 'dikeHYD.mat';

% load arrival data;
filter = find(dykHYD.nsta > 5);
dykHYD = keeprowsarray(dykHYD,filter);
dykOBS = keeprowsarray(dykOBS,filter);
aa = strmatch('NW',dykHYD.comm)
dykHYD = delrowsarray(dykHYD,aa)
dykOBS = delrowsarray(dykOBS,aa)

%% STATISTICAL ANALYSIS OF EPICENTER LOCATIONS & AZIMUTHAL DIFFERENCES
[epi_diff,az] = distance(dykOBS.lat,dykOBS.lon,dykHYD.lat,dykHYD.lon);
epi_diff = deg2km(epi_diff);
tdelay = sort(abs(dykOBS.time - dykHYD.time))*86400;

% Compute Quantiles for all events & Estimate the mean at 95% confidence
interval
mean_epidiff = mean(bootstrp(10000,@mean,epi_diff))
mean_tdelay = mean(bootstrp(10000,@mean,tdelay))
mean_mag = mean(bootstrp(10000,@mean,dykOBS.ML))
mean_depth = mean(bootstrp(10000,@median,dykOBS.depth))
std_depth = mean(bootstrp(10000,@std,dykOBS.depth))

confmean_epidiff =
bootci(10000,{@mean,epi_diff},'alpha',0.05,'type','bca') % BCA confidence
limits
confmean_tdelay = bootci(10000,{@mean,tdelay},'alpha',0.05,'type','bca') %
BCA confidence limits
confmean_mag = bootci(10000,{@mean,dykOBS.ML},'alpha',0.05,'type','bca') %
BCA confidence limits
confmean_depth =
bootci(10000,{@median,dykOBS.depth},'alpha',0.05,'type','bca') % BCA
confidence limits

Q25 = mean(bootstrp(10000,@quantile,epi_diff,(0.25)))
```

```
lessQ25 = length(find(epi_diff <= Q25));
Q50 = mean(bootstrp(10000,@quantile,epi_diff,(0.50)))
lessQ50 = length(find(epi_diff <= Q50));
Q75 = mean(bootstrp(10000,@quantile,epi_diff,(0.75)))
lessQ75 = length(find(epi_diff <= Q75));
Q975 = mean(bootstrp(10000,@quantile,epi_diff,(0.975)))
lessQ975 = length(find(epi_diff <= Q975));
Q = [Q25,Q50,Q75,Q975]

%% Directional Statistics for off-axis swarms

figure;
whitebg('w')
Xr = sum(sind(az))/length(az)
Yr = sum(cosd(az))/length(az)
naz = numel(az)
% Resultant length
Res_length = sqrt(Xr^2 + Yr^2) % Overall mean resultant length

% Mean azimuth
X_theta = asind(Xr/Res_length)% since X is positive
Mean_az = acosd(Yr/Res_length)
std_az = std(acosd(Yr/Res_length))
%mean_az = atand(Xr/Yr) % mean azimuth

circ_var = 100*(1-Res_length) % Circular variance

% Schuster Test
[p, meanaz,meanReslength] = schuster_plus(az)
numb = find(az>=60 & az <=210);
% Compute confidence in the mean
conf_mean = rad2deg(circ_confmean(deg2rad(az),0.05))

Results = [naz Q p meanaz meanReslength conf_mean circ_var]

%% Azimuthal distribution of All Events

figure;
az_rad = az*pi/180;
[x,y] = pol2cart(az_rad,epi_diff);
compass(x,y);view([90,-90]);
title('Compass plot of Epicentral difference of the swarm at
20.5S,176W','fontsize',24);
grid on

% percentage shifted to southwest
numb = numel(find(az>=60 & az <=210));
percntage_displacement = (138/191)*100

%% Order of arrival
order = find(strncmpi(dykHYD.order,'CBDEYM',6))
length_order = numel(order)

% Acoustic source level Vs Magnitude Vs Stations
```

```
figure;
gscatter(dykOBS.ML,dykHYD.SL,dykHYD.nsta-3,'crmg','.',siz);hold on
xlabel('Local Earthquake Magnitude (ML)','fontsize',16)
ylabel('Acoustic Source Level (dB re 1 uPa@ 1m)','fontsize',16)
grid on
```

Appendix 4 - UNCERTAINTY ANALYSIS OF OFF-AXIS SWARMS

```
% load the volcanic swarm at 20.50
load dikeOBS.mat; % seismic events
load dikeHYD.mat; % Acoustic events

filter = find(dykHYD.nsta > 5);
dykHYD = keeprowsarray(dykHYD,filter);
dykOBS = keeprowsarray(dykOBS,filter);

%% Error Ellipse

[epi_diff,az] = distance(dykOBS.lat,dykOBS.lon,dykHYD.lat,dykHYD.lon);
epi_diff = deg2km(epi_diff);

%8. Plot the ellipse
figure;
%axesm mercator
plot(dykOBS.lon,dykOBS.lat,'r+');hold on
plot(dykHYD.lon,dykHYD.lat,'k+');hold on
dykOBS.errhor = km2deg(dykOBS.errhor);

dykHYD.errhor = 2*deg2km(mean(dykHYD.lat))
% dykOBS.errver = 2.4*km2deg(dykOBS.errver);
% find the semi-major axis
n = length(dykOBS.lat)
for i = 1:length(dykOBS.errhor);

    major(i) = 2.4*dykOBS.errhor(i);
    minor(i) = 2.4*dykOBS.errhor(i);
    ecc(i) = axes2ecc(major(i),minor(i)); % compute the eccentricity of
the ellipse
    [elat,elon] = ellipse1(dykOBS.lat(i),dykOBS.lon(i),[major(i),
ecc(i)]);
    plot(elon,elat,'b');hold on

    % Find which twave epicenters fall into the seismic error ellipse
    match(i) = inpolygon(dykHYD.lat(i),dykHYD.lon(i),elat,elon);

    % Second way to find if twave epicenter falls in seismic epicenter
    criterion(i) = (2.4*dykOBS.errhor(i))/km2deg(epi_diff(i));


end
%7. Plot the vector between both catalogs
```

```
for i = 1: n;
    plot([dykOBS.lon(i),dykHYD.lon(i)],[dykOBS.lat(i),dykHYD.lat(i)],'-
k');
end

xlabel('Longitude','fontsize',16)
ylabel('Latitude','fontsize',16)
title('Earthquake Standard Error distribution at 95%
confidence','fontsize',16)
grid on

% Compute mean horizontal error
mean_errhor = deg2km(mean(dykOBS.errhor))

% Percentage in error ellipse
% Find where there's a match
P = length(find(match ==1))
Pcntg_in = (P/n)*100

%% ERROR BAR PLOT

figure;
grid on;
herrorbar(dykHYD.lon,dykHYD.lat,dykHYD.errlon,'.r');hold on
errorbar(dykHYD.lon,dykHYD.lat,dykHYD.errlat,'.b');hold on
legend(' ','error in longitude','error in latitude')
xlabel('Longitude','fontsize',16)
ylabel('Latitude','fontsize',16)
grid on

figure;
errorbar(dykOBS.lon,dykOBS.lat,dykOBS.errhor,'.k');hold on
errorbar(dykHYD.lon,dykHYD.lat,dykHYD.errlat,'.b');hold on
grid on
legend('Error in Latitude - Seismic',' Error in Latitude - T-wave')
xlabel('Longitude','fontsize',16)
ylabel('Latitude','fontsize',16)

%% ERROR ANALYSIS
%% ERROR BAR PLOT

figure;
errorbar(dykHYD.lon,dykHYD.lat,dykHYD.errlon,'.r');hold on
errorbar(dykHYD.lon,dykHYD.lat,dykHYD.errlat,'.b');hold on
errorbar(dykOBS.lon,dykOBS.lat,dykOBS.errhor,'.k');hold on

% Error in epicentral parameters
close all

lat_diff = deg2km(dykOBS.lat - dykHYD.lat); %Error in latitude
figure;subplot(2,1,1);stem(lat_diff)
ylabel('Difference in Latitude (km)','fontsize',16)
xlabel('# of Events','fontsize',16)
grid on
```

```
lon_diff = deg2km(dykOBS.lon - dykHYD.lon); %Error in latitude
subplot(2,1,2);stem(lon_diff)
ylabel('Difference in Longitude (km)','fontsize',16)
xlabel('# of Events','fontsize',16)
grid on

%% Error in latitude

figure;
hist(dykOBS.lat);
hold on;
%//make data1 red
%//get the handle of the bars in a histogram
h = findobj(gca,'Type','patch');
%//color of the bar is red and the color of the border
%// of the bar is white!
set(h,'FaceColor','r','EdgeColor','k');
%//data 2 use default color!
hist(dykHYD.lat);
xlabel('Latitude','fontsize',16)
ylabel('# of Events','fontsize',16)
title('Distribution of Events along strike','fontsize',16)
legend('seismic','hydoacoustic')

%% Error in Longitude

figure;
hist(dykOBS.lon);
hold on;
%//make data1 red
%//get the handle of the bars in a histogram
h = findobj(gca,'Type','patch');
%//color of the bar is red and the color of the border
%// of the bar is white!
set(h,'FaceColor','r','EdgeColor','k');
%//data 2 use default color!
hist(dykHYD.lon);
xlabel('Latitude','fontsize',16)
ylabel('# of Events','fontsize',16)
title('Distribution of Events along strike','fontsize',16)
legend('seismic','hydoacoustic')

%% Distribution of events along strike

figure;
hist(dykOBS.time,20);
hold on;
%//make data1 red
%//get the handle of the bars in a histogram
h = findobj(gca,'Type','patch');
%//color of the bar is red and the color of the border
%// of the bar is white!
set(h,'FaceColor','r','EdgeColor','k');
```

```
%//data 2 use default color!
hist(dykHYD.time,20);
xlabel('Latitude','fontsize',16)
ylabel('# of Events','fontsize',16)
title('Distribution of Events along strike','fontsize',16)
legend('seismic','hydoacoustic')
```

APPENDIX 5 – STATISTICAL ANALYSIS OF THE EVENTS ALONG AXIS

```
%% load origin data
load 'axis_OBS.mat';
load 'axis_HYD.mat';

% load arrival data;
filter = find(axisHYD.nsta > 5);
axisHYD = keeprowsarray(axisHYD,filter);
axisOBS = keeprowsarray(axisOBS,filter);
aa = strmatch('NW',axisHYD.comm)
axisHYD = delrowsarray(axisHYD,aa)
axisOBS = delrowsarray(axisOBS,aa)

table = [axisOBS.lat,axisOBS.lon];

% Write OBS lat and lon to file
file = 'OBSlatlon.xls';
xlswrite(file,table)

%Write hydrophone lat lon to file
file = 'hydlatlon.txt';
xlswrite(file,[axisHYD.lat,axisOBS.lon])

%% STATISTICAL ANALYSIS OF EPICENTER LOCATIONS & AZIMUTHAL DIFFERENCES
[epi_diff,az] = distance(axisOBS.lat,axisOBS.lon,axisHYD.lat,axisHYD.lon);
epi_diff = deg2km(epi_diff);

% Origin time difference
tdelay = sort((axisHYD.time - axisOBS.time))*86400;
figure;

% HISTOGRAM OF THE TIME DELAY FOR VALID OBS & AUH MATCHES
whitebg('w')
%tdelay = abs(tdelay)
bin = min(tdelay):0.4:max(tdelay);
[freq,bin]=hist(tdelay,bin);
bar(bin,freq);hold on
grid on;
xm = [3.0,3.0];ym =[0,40];
plot(xm,ym,'k')
axis([min(tdelay) 5.5 0 40])
h = findobj(gca,'Type','patch');
set(h,'Facecolor','w','Edgecolor','r');
xlabel('Origin time difference (secs)','fontsize',16)
ylabel('Frequency','fontsize',16)
```

```
title('Origin time delay btw Seismic & Tphase derived
epicenters','fontsize',16)
legend('mean delay = 3.0s and std = 1.0s', 'Location','Northeast');


%% STATISTICAL ANALYSIS OF EPICENTER LOCATIONS & AZIMUTHAL DIFFERENCES

% Compute Quantiles for all events & Estimate the mean at 95% confidence
interval
mean_epidiff = mean(bootstrp(10000,@mean,epi_diff))
mean_tdelay = mean(bootstrp(10000,@mean,tdelay))
mean_mag = mean(bootstrp(10000,@mean,axisOBS.ML))
mean_depth = mean(bootstrp(10000,@median,axisOBS.depth))
std_depth = mean(bootstrp(10000,@std,axisOBS.depth))

confmean_epidiff =
bootci(10000,{@mean,epi_diff},'alpha',0.05,'type','bca') % BCA confidence
limits
confmean_tdelay = bootci(10000,{@mean,tdelay},'alpha',0.05,'type','bca') %
BCA confidence limits
confmean_mag = bootci(10000,{@mean,axisOBS.ML},'alpha',0.05,'type','bca')
% BCA confidence limits
confmean_depth =
bootci(10000,{@median,axisOBS.depth},'alpha',0.05,'type','bca') % BCA
confidence limits


Q25 = mean(bootstrp(10000,@quantile,epi_diff,(0.25)))
lessQ25 = length(find(epi_diff <= Q25));
Q50 = mean(bootstrp(10000,@quantile,epi_diff,(0.50)))
lessQ50 = length(find(epi_diff <= Q50));
Q75 = mean(bootstrp(10000,@quantile,epi_diff,(0.75)))
lessQ75 = length(find(epi_diff <= Q75));
Q975 = mean(bootstrp(10000,@quantile,epi_diff,(0.975)))
lessQ975 = length(find(epi_diff <= Q975));
Q = [Q25,Q50,Q75,Q975]

%% Directional Statistics of on-axis swarms

figure;
whitebg('w')
Xr = sum(sind(az))/length(az)
Yr = sum(cosd(az))/length(az)
naz = numel(az)
% Resultant length
Res_length = sqrt(Xr^2 + Yr^2) % Overall mean resultant length

% Mean azimuth
X_theta = asind(Xr/Res_length)% since X is positive
Mean_az = acosd(Yr/Res_length)
std_az = std(acosd(Yr/Res_length))
%mean_az = atand(Xr/Yr) % mean azimuth

circ_var = 100*(1-Res_length) % Circular variance
```

```
% Schuster Test
[p, meanaz,meanReslength] = schuster_plus(az)
if meanaz < 0
    meanaz = meanaz + 360
end
%numb = find(az>=180 & az <=360);
% Compute confidence in the mean
conf_mean = rad2deg(circ_confmean(deg2rad(az),0.05))

Rayleigh_test = length(az)*Res_length^2

%Results_evl2 = [nev_less2 Ql25 Ql50 Ql90 p_l2 meanaz_l2 conf_meanl2
meanResl2 circ_varl2]
%Results_evgt2 = [nev_gtr2 Qg25 Qg50 Qg90 p_g2 meanaz_g2 conf_meang2
meanResg2 circ_varg2]
Results = [naz Q p meanaz meanReslength conf_mean circ_var]

%% COMPASS PLOT - Azimuthal distribution of onaxis swarms

figure;
az_rad = az*pi/180;
[x,y] = pol2cart(az_rad,epi_diff);
compass(x,y);view([90,-90]);
%title('Compass plot of Epicentral difference of the swarm at
20.5S,176W','fontsize',24);
grid on

% percentage shifted to southwest
numb = (find(az>=180 & az <=360));
percntage_displacement = (138/191)*100

%% %% Order of arrival
order = find(strncmpi(axisHYD.order,'MLC',1))
length_order = numel(order)

% Acoustic source level Vs Magnitude Vs Stations
figure;
gscatter(axisOBS.ML,axisHYD.SL,axisHYD.nsta-3,'crmg','.',siz);hold on
xlabel('Local Earthquake Magnitude (ML)','fontsize',16)
ylabel('Acoustic Source Level (dB re 1 uPa@ 1m)','fontsize',16)
grid on
```

APPENDIX 6 - UNCERTAINTY ANALYSIS OF EVENTS ALONG-AXIS

```
%% UNCERTAINTY ANALYSIS OF EVENTS ALONG-AXIS

% load the volcanic swarm at 20.50
load axis_OBS.mat; % seismic events
load axis_HYD.mat; % Acoustic events

filter = find(axisHYD.nsta > 5);
axisHYD = keeprowsarray(axisHYD,filter);
axisOBS = keeprowsarray(axisOBS,filter);
%
% load the volcanic swarm at 20.50
load dikeOBS.mat; % seismic events
load dikeHYD.mat; % Acoustic events

filter = find(dykHYD.nsta > 5);
dykHYD = keeprowsarray(dykHYD,filter);
dykOBS = keeprowsarray(dykOBS,filter);
%% Error Ellipse

[epi_diff,az] = distance(axisOBS.lat,axisOBS.lon,axisHYD.lat,axisHYD.lon);
epi_diff = deg2km(epi_diff);

tdelay = sort(abs(axisHYD.time - axisOBS.time))*86400;

Axxis = load('~/Documents/MATLAB/rd_antelope/d_misc/neovolcanic.xyz');
%8. Plot the ellipse
figure;
whitebg('w')
%axesm mercator
plot(axisOBS.lon,axisOBS.lat,'r+');hold on
plot(axisHYD.lon,axisHYD.lat,'k+');hold on
plot(-(360-Axxis(:,1)),Axxis(:,2),'r');hold on
axis([-177 -175 -22 -18])
axisOBS.errhor = km2deg(axisOBS.errhor);

%axisHYD.errhor = 2*deg2km(mean(axisHYD.lat))
% axisOBS.errver = 2.4*km2deg(axisOBS.errver);
% find the semi-major axis
n = length(axisOBS.lat)
for i = 1:length(axisOBS.errhor);

    major(i) = 2.4*axisOBS.errhor(i);
    minor(i) = 2.4*axisOBS.errhor(i);
    ecc(i) = axes2ecc(major(i),minor(i)); % compute the eccentricity of
the ellipse
    [elat,elon] = ellipse1(axisOBS.lat(i),axisOBS.lon(i),[major(i),
ecc(i)]);
    plot(elon,elat,'b');hold on

    % Find which twave epicenters fall into the seismic error ellipse
    match(i) = inpolygon(axisHYD.lat(i),axisHYD.lon(i),elat,elon);
```

```
    % Second way to find if twave epicenter falls in seismic epicenter
    criterion(i) = (2.4*axisOBS.errhor(i))/km2deg(epi_diff(i));


end
%7. Plot the vector between both catalogs
for i = 1: n;

plot([axisOBS.lon(i),axisHYD.lon(i)],[axisOBS.lat(i),axisHYD.lat(i)],'-
k');
end

xlabel('Longitude','fontsize',16)
ylabel('Latitude','fontsize',16)
%title('Earthquake Standard Error distribution at 95%
confidence','fontsize',16)
grid on

% Compute mean horizontal error
mean_errhor = deg2km(mean(axisOBS.errhor))

% Percentage in error ellipse
% Find where there's a match
P = length(find(criterion >=1))
Pcntg_in = (P/n)*100

%% ERROR BAR PLOT
axisOBS.errhor = 2.4*axisOBS.errhor;
HYDerrhor = 1.96*axisHYD.errlon;

% Estimate the mean error estimate at 95% confidence interval
meanOBSerror = mean(bootstrp(10000,@mean,deg2km(axisOBS.errhor./2.4)))
meanHYDerror = mean(bootstrp(10000,@mean,deg2km(HYDerrhor./1.96)))

% Estimate 95%confidence interval error estimate
confmeanHYDerror=bootci(10000,{@mean,deg2km(HYDerrhor)},'alpha',0.05,'type
','bca') % BCA confidence limits
confmeanOBSerror=bootci(10000,{@mean,deg2km(axisOBS.errhor)},'alpha',0.05,
'type','bca') % BCA confidence limits


diff = (axisHYD.errlon - axisHYD.errlat);
fix = find(diff<0);
for i = 1:HYDerrhor;
if diff<0
   HYDerrhor(i) = 1.96*(axisHYD.errlat(i))
end
end

figure;
whitebg('w')
grid on;
Axxis = load('~/Documents/MATLAB/rd_antelope/d_misc/neovolcanic.xyz');
plot(-(360-Axxis(:,1)),Axxis(:,2),'k');hold on
```

```
herrorbar(axisHYD.lon,axisHYD.lat,1.96*axisHYD.errlon,'.r');hold on
errorbar(axisHYD.lon,axisHYD.lat,1.96*axisHYD.errlat,'.b');hold on
legend('Spreading Centers','error in longitude','error in latitude')
xlabel('Longitude','fontsize',16)
ylabel('Latitude','fontsize',16)
axis([-177 -175 -22.25 -18.5])
grid on

figure;
whitebg('w')
Axxis = load('~/Documents/MATLAB/rd_antelope/d_misc/neovolcanic.xyz');
plot(-(360-Axxis(:,1)),Axxis(:,2),'k');hold on


errorbar(axisOBS.lon,axisOBS.lat,axisOBS.errhor,'.k');hold on
errorbar(axisHYD.lon,axisHYD.lat,HYDerrhor,'.b');hold on
%plot(axisHYD.lon,axisHYD.lat,'.r');hold on
grid on
legend('spreading Centers','- Seismic','- T-wave')
xlabel('Longitude','fontsize',16)
ylabel('Latitude','fontsize',16)
axis([-177 -175 -22.25 -18.5])

% Finding the overlap region
overlap = numel(find(deg2km(HYDerrhor)>=1.86 &
deg2km(axisOBS.errhor)<=2.44))
return
%% Acoustic source level Vs Magnitude
whitebg
figure;whitebg('w')
plot(axisOBS.ML,axisHYD.SL,'.r','MarkerSize',12);hold on
herrorbar(axisOBS.ML,axisHYD.SL,axisOBS.MLste,'.r');hold on
xlabel('Local Earthquake Magnitude','fontsize',16)
ylabel('Acoustic Source Level (dB re 1 uPa@ 1m)','fontsize',16)
title('Source Level Vs Seismic Magnitude ','fontsize',16)

% fit straight line to ASL-ML
[P, S] = polyfit(axisOBS.ML,axisHYD.SL,1)
[pred delta]= polyval(P,axisOBS.ML,S)
plot(axisOBS.ML,pred,'-b','LineWidth',2);
% Obtain confidence interval
%plot(axisOBS.ML,pred+delta,'--k');hold on; plot(axisOBS.ML,pred-delta,'--
k');
legend('Slope = 14.97 & intercept = 175.47','Location','Northeast')

%
for i = 1:numel(epi_diff)
    if epi_diff(i) <=2
        epi_diff(i) = 2
    elseif epi_diff(i) >2 & epi_diff(i)<=4
        epi_diff(i) = 4
    else
        epi_diff(i) = 6
    end
```

```
end

figure;gscatter(axisOBS.ML,axisHYD.SL,epi_diff)
%% Residual Analysis

% Calculate the R-squared
residual = axisHYD.SL - pred;% compute the residual values
SSresidual = sum(residual.^2);% compute the residual sum of squares
SStotal = (length(axisHYD.SL) - 1)* var(axisHYD.SL); % comoute total sum
of squares
rsquare = 1 - SSresidual/SStotal % compute the R-squared
Adj_rsquare = 1 - SSresidual/SStotal * (length(axisHYD.SL) -
1)/(length(axisHYD.SL) - length(P))

figure;
stem(axisOBS.ML,residual,'.r');hold on
grid on
xlabel('Seismic Magnitude','fontsize',16)
ylabel('Residuals (Source Level)','fontsize',16)
legend('residuals (dB)')

%% Histogram distribution of Acoustic Source Level
figure;
whitebg('w')
range = min(axisHYD.SL):1:max(axisHYD.SL);%define range of data
[freq,bin] = hist(axisHYD.SL,range);% generate frequencies and bins
% Regular frequency magnitude distribution
Rfreq = freq(length(freq):-1:1);
% Cumulative frequency magnitude distribution
Cfreq = cumsum(freq(length(freq):-1:1));
Xaxis = max(axisHYD.SL):-1:min(axisHYD.SL);% define axis values and limits
stairs(Xaxis,Cfreq,'k');hold on
%bar(Xaxis,Cfreq,'w','EdgeColor','k');hold on;
stairs(range,freq,'r');
xlabel('Acoustic SOurce Level (dB re 1 uPa@ 1m)','fontsize',16)
ylabel('Number of Events','fontsize',16)
grid on
%% Difference in Epicentral Parameters
%% ONAXIS
lat_diff = deg2km(axisOBS.lat - axisHYD.lat); %Error in latitude
figure;
whitebg('w')
subplot(2,1,1);stem(lat_diff)
ylabel('Difference in Latitude (km)','fontsize',16)
xlabel('# of Events','fontsize',16)

% Compute the standard error in latitudinal difference
std_errlataxis=std(lat_diff)/sqrt(length(lat_diff)) % standard error of
the mean
grid on

lon_diff = deg2km(axisOBS.lon - axisHYD.lon); %Error in latitude
subplot(2,1,2);stem(lon_diff)
ylabel('Difference in Longitude (km)','fontsize',16)
```

```
xlabel('# of Events','fontsize',16)
% Compute the standard error in longitudinal difference
std_errlonaxis=std(lon_diff)/sqrt(length(lon_diff)) % standard error of
the mean
grid on

%1. Compute epi_diff stats
avg_epdiff = mean(bootstrp(2000,@mean,epi_diff))
ci_epidiff = bootci(2000,@mean,epi_diff)
std_epi_diff = mean(bootstrp(2000,@std,epi_diff))
stderr_epidiff = std(bootstrp(2000,@mean,epi_diff))

%2. Compute tdelay stats
avg_tdelay = mean(bootstrp(2000,@mean,tdelay))
ci_tdelay = bootci(2000,@mean,tdelay)
std_tdelay = mean(bootstrp(2000,@std,tdelay))
stderr_tdelay = std(bootstrp(2000,@mean,tdelay))

%3. Compute Magnitude stats
avg_axisOBS.ML = mean(bootstrp(2000,@mean,axisOBS.ML))
ci_axisOBSML = bootci(2000,@mean,axisOBS.ML)
std_axisOBSML = mean(bootstrp(2000,@std,axisOBS.ML))
stderr_axisOBSML = std(bootstrp(2000,@mean,axisOBS.ML))

%4. Compute Depth Stats
avg_axisOBSdepth = mean(bootstrp(2000,@median,axisOBS.depth))
ci_axisOBSdepth = bootci(2000,@median,axisOBS.depth)
std_axisOBSdepth = mean(bootstrp(2000,@std,axisOBS.depth))
stderr_axisOBSdepth = std(bootstrp(2000,@mean,axisOBS.depth))

%% OFF-AXIS
lat_diff = deg2km(dykOBS.lat - dykHYD.lat); %Error in latitude
figure;
whitebg('w')
subplot(2,1,1);stem(lat_diff)
ylabel('Difference in Latitude (km)','fontsize',16)
xlabel('# of Events','fontsize',16)
% Compute the standard error in latitudinal difference
std_errlatdyk=std(lat_diff)/sqrt(length(lat_diff)) % standard error of the
mean
grid on

lon_diff = deg2km(dykOBS.lon - dykHYD.lon); %Error in latitude
subplot(2,1,2);stem(lon_diff)
ylabel('Difference in Longitude (km)','fontsize',16)
xlabel('# of Events','fontsize',16)
% Compute the standard error in longitudinal difference
std_errlondyk=std(lon_diff)/sqrt(length(lon_diff)) % standard error of the
mean
grid on

%% OFF-AXIS

[epi_diff,az] = distance(dykOBS.lat,dykOBS.lon,dykHYD.lat,dykHYD.lon);
```

```
epi_diff = deg2km(epi_diff);

tdelay = sort(abs(dykHYD.time - dykOBS.time))*86400;

%1. Compute epi_diff stats
avg_epdiff = mean(bootstrp(2000,@mean,epi_diff))
ci_epidiff = bootci(2000,@mean,epi_diff)
std_epi_diff = mean(bootstrp(2000,@std,epi_diff))
stderr_epidiff = std(bootstrp(2000,@mean,epi_diff))

%2. Compute tdelay stats
avg_tdelay = mean(bootstrp(2000,@mean,tdelay))
ci_tdelay = bootci(2000,@mean,tdelay)
std_tdelay = mean(bootstrp(2000,@std,tdelay))
stderr_tdelay = std(bootstrp(2000,@mean,tdelay))

%3. Compute Magnitude stats
avg_dykML = mean(bootstrp(2000,@mean,dykOBS.ML))
ci_dykOBSML = bootci(2000,@mean,dykOBS.ML)
std_dykML = mean(bootstrp(2000,@std,dykOBS.ML))
stderr_dykML = std(bootstrp(2000,@mean,dykOBS.ML))

%4. Compute Depth Stats
avg_dykOBSdepth = mean(bootstrp(2000,@median,dykOBS.depth))
ci_dykOBSdepth = bootci(2000,@median,dykOBS.depth)
std_dykOBSdepth = mean(bootstrp(2000,@std,dykOBS.depth))
stderr_dykOBSdepth = std(bootstrp(2000,@mean,dykOBS.depth)
```